

STRUCTURAL ANALYSIS OF POWER AUGMENTED GUIDE

VANE FOR THE VERTICAL AXIS WIND TURBINE

AMIN KAZEMZADEH

FACULTY OF ENGINEERING

UNIVERSITY OF MALAYA

KUALA LUMPUR

2012

**STRUCTURAL ANALYSIS OF POWER AUGMENTED GUIDE
VANE FOR THE VERTICAL AXIS WIND TURBINE**

AMIN KAZEMZADEH

**DISSERTATION SUBMITTED IN PARTIAL FULFILLMENT
OF THE REQUIREMENT
FOR THE DEGREE OF MASTER OF ENGINEERING**

FACULTY OF ENGINEERING

UNIVERSITY OF MALAYA

KUALA LUMPUR

2012

ABSTRACT

This report illustrates the static structural analysis of the power augmented guide vane (PAGV) performed by the finite element (FE) method. The results obtained can be used to apply the PAGV in the real environmental conditions. As part of the equatorial regions, Malaysia experiences low and unsteady wind speed. Most of the areas experience a wind speed, which is lower than 4 m/s for most hours. Thus, the PAGV is designed to overcome the inferior aspect of low wind speed in Malaysia by guiding and increasing the speed (almost 1.7 times) of high altitude free-stream wind from all directions before entering the wind turbine. The vertical axis wind turbine (VAWT) was chosen and enclosed by the PAGV, so this can minimize the current problems of wind energy such as bird strike, the noise pollution and electromagnetic interference. In fact, the PAGV is a multipurpose appliance, which the solar panel can be laid on its top surface. It can also collect the rain water by directing the rain water to flow towards the center of the system where the water is stored in a storage tank for general use. In this research, the static structural analysis of the PAGV has been carried out by using ANSYS software. The pressure distribution and wind speed that flows through the PAGV have been analyzed and simulated by using ANSYS Fluent software. The simulation results for the PAGV of the wind speed of 60 m/s showed minimum safety factor of 1.7 for the specified materials. However, the simulation showed that a disagreeable large deflection occurred at the middle of each vanes of the PAGV, which reaches maximum 9.46 mm. By introducing a new support system, an attempt has been done to improve the initial design. Also, the problem of large deflection is expected be removed in the proposed support system.

ABSTRAK

Kajian ini menunjukkan struktur statik analisis *power augmented guide vane* (PAGV) melalui FEM. Keputusan yang diperoleh boleh digunakan untuk mengaplikasikan PAGV pada kondisi persekitaran yang sebenar. Sebagai Negara yang berada di kawasan khatulistiwa, Malaysia mempunyai kelajuan angin yang rendah dan kebanyakan kawasan mempunyai kelajuan angin yang lebih rendah dari 4 m/s. Oleh itu, PAGV direka untuk mengatasi kelajuan angin yang rendah di Malaysia dengan memberi panduan dan menaikkan kelajuan (hampir 1.7 kali) tinggi altitude arus angin bebas dari semua arah sebelum memasuki turbin angin. Paksi tegak turbin angin dipilih dan disertakan dengan PAGV supaya ia dapat mengurangkan masalah kuasa angin yang sedia seperti serangan burung, pengurangan pencemaran bunyi dan gangguan elektromagnet. Sebenarnya PAGV ialah perkakas yang serbaguna, di mana panel sel solar boleh diletakkan di atasnya. Ia juga boleh mengumpulkan air hujan dengan mengalirkan air hujan ke pusat sistem di mana air disimpan dalam tangki untuk kegunaan umum. Dalam penyelidikan ini, analisis struktur statik PAGV telah dikendalikan menggunakan perisian ANSYS. Pengagih hentakan dan kelajuan angin yang mengalir melalui PAGV telah dianalisis dan disimulasi menggunakan perisian ANSYS. Keputusan simulasi PAGV untuk kelajuan angin sebanyak 60 m/s menunjukkan nilai minimum 1.7 iaitu faktor keselamatan bagi bahan tertentu. Walaubagaimanapun, simulasi menunjukkan defleksi yang besar berlaku di bahagian tengah setiap *vane*, PAGV, di mana ia menghampiri nilai maksimum 9.46 mm. Dengan mengenalkan sistem sokongan yang baru, satu pencarian telah dijalankan untuk membaik pulih rekaan yang lama. Selain itu, masalah defleksi yang besar juga di jangka dapat di hapuskan dengan sistem sokongan ini.

UNIVERSITI MALAYA

ORIGINAL LITERARY WORK DECLARATION

Name of Candidate: AMIN KAZEMZADEH (I.C/Passport No: R19246790)
Registration/Matric No: KGH070005
Name of Degree: MASTER OF ENGINEERING (MECHANICAL)
Title of Project Paper/Research Report/Dissertation/Thesis "this Work":
STRUCTURAL ANALYSIS OF POWER AUGMENTED GUIDE VANE FOR THE
VERTICAL AXIS WIND TURBINE

FIELD OF STUDY:

I do solemnly and sincerely declare that:

- (1) I am the sole author/writer of this Work;
- (2) This Work is original;
- (3) Any use of any work in which copyright exists was done by way of fair dealing and for permitted purposes and any excerpt or extract from, or reference to or reproduction of any copyright work has been disclosed expressly and sufficiently and the title of the Work and its authorship have been acknowledged in this Work;
- (4) I do not have any actual knowledge nor do I ought reasonably to know that the making of this work constitutes an infringement of any copyright work;
- (5) I hereby assign all and every rights in the copyright to this Work to the University of Malaya ("UM"), who henceforth shall be owner of the copyright in this Work and that any reproduction or use in any form or by any means whatsoever is prohibited without the written consent of UM having been first had and obtained;
- (6) I am fully aware that if in the course of making this Work I have infringed any copyright whether intentionally or otherwise, I may be subject to legal action or any other action as may be determined by UM.

Candidate's Signature

Date

Subscribed and solemnly declared before,

Witness's Signature

Date

Name:

Designation:

Acknowledgements

First, I would like to express my gratefulness and great thanks to my supervisor, Dr. Chong Wen Tong, for giving me the opportunity to carry out this project with title of “structural analysis of power augmented guide vane for the vertical axis wind turbine”. His constructive comments, guidance and suggestions are appreciated.

Besides that, I want to thank my partners and offer my regards and blessings to those supported me in any respect during the completion of the project.

University of Malaysia

Contents

ABSTRACT	i
Acknowledgements	iv
CHAPTER1	1
1.1 Research Background	1
1.2 Problem Statement	2
1.3 Objectives and Aims of the Research	2
1.4 Methodology	3
2 CHAPTER 2	5
2.1 Vertical and Horizontal Wind Turbine	5
2.1.1 Diffuser Augmented Wind Turbine	10
2.1.2 Climate Effects	13
2.2 Siting wind turbine in urban area	13
2.3 Guide Vane	15
2.4 Structural Analysis	16
2.5 Numerical Studies	17
2.6 Material studies	19
3 CHAPTER 3	21
3.1 Basic Definitions	21
3.1.1 Bernoulli's Principle	23
3.1.2 Venturi Effect	23
3.2 Computational Fluid Dynamics (CFD)	24
3.2.1 Discretization Methods	25
3.2.2 Solution Convergence	29
3.2.3 Nonlinearity	29
3.2.4 Turbulence Models	30
3.3 $k-\varepsilon$ Turbulence Model	33
3.5 Boundary Conditions	35
3.6 Finite Element Method	36
3.7 Failure Theories	38
3.8 Failure Theories	40
4 CHAPTER 4	41
4.1 Research Background	41
4.2 Initial Design	43
4.3 Material Properties	46
4.4 Support Configuration	47

4.5	Computational Scope	49
4.5.1	Contours of Pressure	50
4.5.2	Wind Domain	50
4.5.3	Boundary Conditions	52
4.5.4	Mesh Process	54
4.5.5	Turbulence Model Parameters	57
4.6	Static Structural Analysis	61
4.6.1	Connecting Analyzing Systems	62
4.6.2	Engineering Data	63
4.6.3	Modeling	64
4.6.4	Analysis Setting	67
4.6.5	Loads and Supports	68
5	CHAPTER 5	71
5.1	Stress Results	72
5.2	Deformation results	73
5.4	Discussion	75
6	CHAPTER 6	80
6.1	Conclusions	80
6.2	Recommendations	80
	References	80
	Appendix A	88
	Appendix B	91

List of Figures

Figure 1.1: Methodology flowchart	4
Figure 2.1: A straight blade H-type Darrieus wind turbine (McHenry, 2010)	7
Figure 2.2: A type of Darrieus (Du et al., 2009)	7
Figure 2.3: Capturing air turbulence generated by vehicles	9
Figure 2.4: The Anara Tower in Dubai (Chino, 2008)	10
Figure 2.5: Vortec 7 project (Paul Gipe, 1998)	11
Figure 2.6: Stages of buckling and post-buckling process in laminate design	18
Figure 3.1: The airfoil with velocity of V_{∞} meets airflow at shown angle of attack	22
Figure 3.2: Continues domain and discrete domain (x_i : Grid point)	25
Figure 3.3: A rectangular cell	27
Figure 3.4: Hierarchy of turbulence models in ANSYS Fluent	33
Figure 3.5: Linear, quadratic and cubic one-dimensional element	37
Figure 3.6: Linear triangular, quadratic triangular and cubic triangular; two-dimensional element	37
Figure 3.7: Linear rectangular, quadrilateral, quadratic quadrilateral and cubic quadrilateral three-dimensional element	37
Figure 3.8: Tetrahedron, Right Prism, Hexahedron; three-dimensional element	37
Figure 3.9: Stress, strain diagram of different materials	40
Figure 4.1: Sectional view of the wind-solar hybrid renewable energy generation system with rainwater collection feature	43
Figure 4.2: The initial PAGV design	44
Figure 4.3: The initial PAGV design together with the supports	45
Figure 4.4: The PAGV-Sectional view	46

Figure 4.5: Side view of a vane and its support	48
Figure 4.6: Sectional view of the PAGV with base support	49
Figure 4.7: Wind domain created for simulation	51
Figure 4.8: Top vie of wind domain	52
Figure 4.9: Boundary condition (velocity inlet and outflow)	53
Figure 4.10: Boundary condition (walls)	54
Figure 4.11: Mesh created for the wind domain	56
Figure 4.12: Three dimensional mesh cut view	56
Figure 4.13: Mesh diversity through the PAGV	57
Figure 4.14: Irritation process	59
Figure 4.15: Contours of pressure on the PAGV obtained by realizable $k-\varepsilon$ model	60
Figure 4.16: Velocity vectors colored by velocity magnitude (m/s) obtained by realizable $k-\varepsilon$ model	60
Figure 4.17: Connecting ANSYS Fluent to ANSYS Static Structural	63
Figure 4.18: Mesh properties window	64
Figure 4.19: Mesh properties	66
Figure 4.20: The PAGV mesh skewness	66
Figure 4.21: The PAGV mesh	67
Figure 4.22: The pressure applied on the PAGV	68
Figure 4.23: Fixed supports of the PAGV	70
Figure 5.1: The equivalent Von-Mises stress	73
Figure 5.2: PAGV deformation	74
Figure 5.3: Strain distribution of the PAGV	75
Figure 5.4: Uniform strength vane	76
Figure 5.5: The deflection support component	77

Figure 5.6: The deflection support ring	77
Figure 5.7: The deflection support ring and attached to the connector disk	78
Figure 5.8: The PAGV and the proposed supports configuration	78
Figure 5.9: The designed support ring	79
Figure A.1: Element number versus maximum stress	88
Figure B.1: Starting the Fluent	88
Figure B.2: Set up the Fluent solver	88
Figure B.3: Selecting the appropriate viscous model	89
Figure B.4: Setting the Realizable $k-\varepsilon$ as the viscous model	89
Figure B.5: Setting the boundary conditions	90
Figure B.6: Define the air velocity magnitude	93
Figure B.7: Choosing the solution schemes	91
Figure B.8: Define under relaxation factors	91
Figure B.9: Define the convergence absolute criteria	92
Figure B.10: Initialize the solution	92
Figure B.11: Transferring the pressure profile to the structural solver	93
Figure B.12: Generating mesh for the PAGV	93
Figure B.13: Project layout	97

List of Tables

Table 3.1: Boundary conditions in ANSYS Fluent	36
Table 3.2: General properties of common structure material (Hibbeler, 2011)	40
Table 4.2: Mechanical properties of the select material	63
Table 5.1: The PAGV material properties	79
Table A.1: Mesh dependency with respect to number of elements	88
Table A.2: Wind speed for all directions based on three second gust wind	89
Table A.3: Terrain and structure factor S_b (BS-6399, Part: 2)	90

University of Malaya

List of Symbols and Abbreviations

Z	Height of the point from reference plane (m)
C_p	Power Coefficient
FR	Resultant force (N)
L	Lift force (N)
D	Drag force (N)
u	Velocity component (m/s)
u_i	Velocity value at point I (m/s)
k	Kinetic energy (J)
ε	Dissipation rate
G_k	The generation of turbulence kinetic energy
G_b	The generation of turbulence kinetic energy due to buoyancy
Y_M	The contribution of the fluctuating dilatation in compressible turbulence to the overall dissipation rate
σ_k	Turbulent Prandtl numbers for k
σ_ε	Turbulent Prandtl numbers for ε
ρ	Density dilatation (Kg/m ³)
S_k	Under-defined source term for k
S_ε	Under-defined source term for ε
μ_t	Turbulent (eddy) viscosity (kg/m.s)
V	Volume of the element (m ³)
E	Young's Modulus (Pa)
$\sigma_{1,2,3}$	Principal stresses (Pa)

S_y Yield strength (Pa)

U_d Distortion energy

University of Malaya

CHAPTER 1

INTRODUCTION

1.1 Research Background

Safe and secure long-term energy with no global or local pollution has encouraged clients and governments to invest in the green energy field. Although there are many renewable technologies commercially available, most of them are still at an early stage of development and not technically mature. These definitely request more research, development and demonstration efforts. Today, wind energy is widely used as the alternative to traditional energy sources. As a matter of fact for many years, wind turbines, especially horizontal axis wind turbines have been used to provide green energy to supply electricity to urban areas.

However, high capital investment and safety issues are formidable to apply these renewable technologies. One of the remedies to reduce the cost of sustainable energy is to innovate and create multipurpose systems. Power augmented guide vane (PAGV) is an innovative wind-solar system, which was designed to overcome the low wind speed in urban areas. The PAGV offers integration of the wind-solar hybrid system with a rainwater harvesting system which can decrease the initial costs. Many structural analysis of the wind turbine blades, rotors and other parts of the wind turbine have been performed by many researchers. A few researchers have studied the structural of the diffusers or ducted wind turbines. However, adding extra equipment to present wind turbine system requires adequate research to be conducted.

1.2 Problem Statement

In order to install wind turbine in urban areas such as on top of high-rise buildings, one of the most important issue is to ensure that it will not endanger people lives. The PAGV increases the safety of the wind turbine by constraining the turbine blades from flying off. But, the PAGV itself must be designed and analyzed in the manner which can tolerate wind storms and high speed winds. Therefore, to design a safer reliable PAGV, it is a crucial issue for using wind turbine in urban areas.

In order to install the wind turbine and guide vane in urban areas regardless of their cost, it is necessary to ensure that using wind turbine in urban areas does not jeopardize the human health. The PAGV itself can be considered as a protection system designed for turbine to be fail-safe. Designing a reliable PAGV which can withstand the above mentioned conditions according to general structural wind loading and safety standards is the matter of interest of this study.

Indeed, safety is the most significant issue for applying the PAGV on the top of the buildings or between the upper levels of the high rise buildings as well as other high structures. Therefore, structural design analysis must be done, in order to prevent any unanticipated accident during the operation of the PAGV.

1.3 Objectives and Aims of the Research

This study presents the static structural analysis of the patented PAGV, in order to assure the reliability and strength of the PAGV under real environmental conditions, particularly on high-rise structures where the wind speed reaches to up 60 m/s. The material used in order to fabricate the PAGV and the minimum overall safety factors of its different parts will be presented. In the process of achieving the main objectives, the pressure profile,

stress and strain of the PAGV will be shown. The aim and objectives of this research can be presented as below:

- To design a safer PAGV to withstand wind speed of 60 m/s according to British standards

1.4 Methodology

In this research, computational fluid dynamics and finite element method were applied to simulate and calculate the wind pressure profile as well as the strength and stress of the proposed PAGV design. The system was designed to overcome the weakness of inconsistent wind in urban areas, which is required for wind turbine operation. The research flow of this study is presented in Figure 1.1.

The required methodology for the study can be presented as below

1. Review of wind turbine systems
2. Review of previous progress of wind turbine and its structural analysis
3. Review of the Finite Element method
4. Review of computational fluid dynamics method
5. To obtain the wind pressure profile using ANSYS Fluent
6. To design the structure of the PAGV
7. To perform structural analysis of the PAGV using ANSYS software
8. Recommendation for the future study

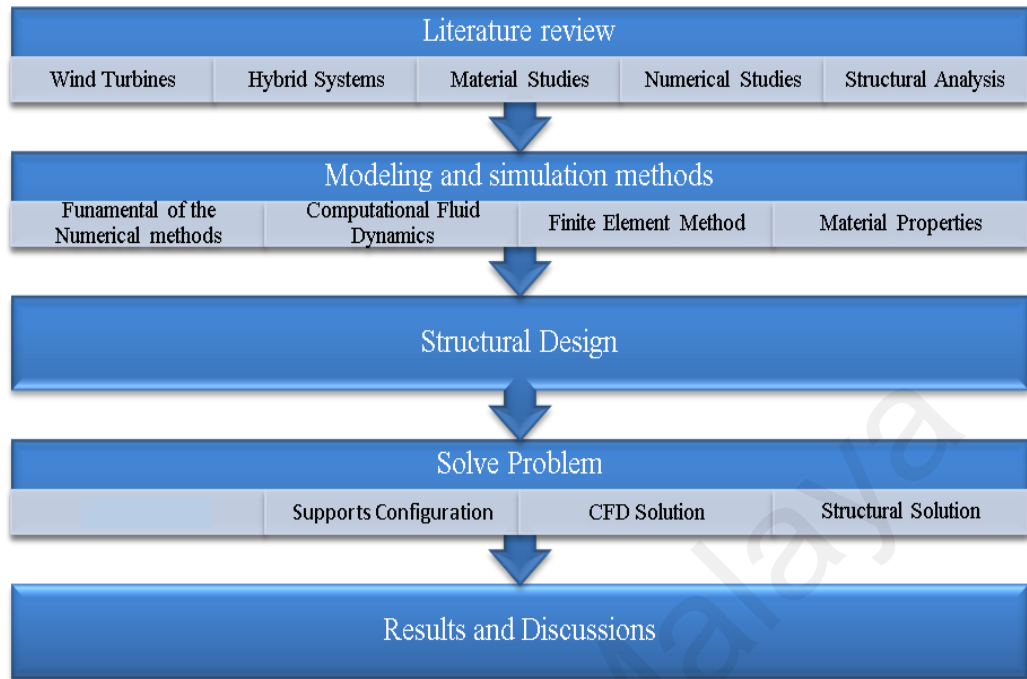


Figure 1.1: Methodology flowchart

University of Malaya

CHAPTER 2

LITERATURE REVIEW

2.1 Vertical and Horizontal Wind Turbine

Wind is the flow of gases on a large scale. Wind power is the transformation of wind energy into electricity as a more utile form by using wind turbines (Gipe, 2004). Today, gradually we are observing that wind turbines are being used in urban areas in order to supply growing energy demands. The earliest reported use of windmills is in Persia during the seventh century (Ackermann, 2005). In Persia, and later on in the other countries, the main use of windmill was to automate the task of grain grinding. However, the first and foremost use of large windmills in the twentieth century was to produce electric power. The first large wind turbine which was set to produce bulk power was installed in Russia at the shore of the Caspian Sea. It was a horizontal axis wind turbine with a 100 kW generator (Burton, 2001). Long afterwards, the federal government of the United States allocated especial budget for the research in the field of wind energy, following the so-called Arab oil crisis of 1973. Since that time, great developments and improvements in wind turbine systems have appeared.

Generally, there are two types of wind turbines, both of which are defined based on the direction of the rotating shaft (axis). They are horizontal axis wind turbines (HAWT) and vertical axis wind turbines (VAWT). The horizontal axis wind turbine is considered a mature technology while the vertical axis is improving rapidly. The first horizontal windmill recorded in historical documents from Persia, Tibet and China around 1000 A.D., these wind mills can be considered as drag devices (Ackermann, 2005).

However, the power coefficient of old drag devices could only reach to a maximum C_p of 0.16 (Gasch, 1982). Nevertheless, developments in the wind turbine industry appears in the different types of vertical and horizontal axis wind turbines such as the Darrieus turbine and the Savonius and so on.

Another main classification is based on the aerodynamic drag and lift characteristics. Modern wind turbines are designed based on aerodynamic lift, which is inspired from aircraft wing shape. Although, applying aerodynamic lift first was used in the horizontal wind turbine, in the Darrieus vertical axis wind turbine, horizontal lift forces were successfully developed on vertical sections of the blades, which turned the whole structure (Cassedy, 2000).

Therefore, the aerodynamic lift-based wind turbines are classified into horizontal-axis and vertical-axis turbines. Operation of the VAWT is independent of the wind direction and its maintenance is easier due to the gearbox and generating machinery, which are placed on the ground. The specific advantages of vertical axis wind turbine concepts are that their simple design has the possibility of housing mechanical and electrical components at the ground level and there is no yaw system (Hau, 2006). However, they have initial disadvantages such as inability to self-start and not being able to control the power output or speed by pitching the rotor blades.

There are two main types of VAWT, which are Darrieus and Savonius. The Savonius rotor was first introduced in 1928 by Finn S.J Savonius (Kentfield, 1996). It is not only a pure drag type turbine, but also the lift can be principally generated at the start up upon to configuration changes. This design of the Darrieus wind turbine was patented by Georges Jean Marie Darrieus, a French aeronautical engineer in 1931 (Miller, Vandome, & McBrewster, 2010). The Darrieus patent practically includes any possible structural

arrangement using vertical airfoils such as Helical, Cycloturbines and Girolmills. Pictures, 2.1 and 2.2 show two different types of the Darrieus wind turbines.



Figure 2.1: A straight blade H-type Darrieus wind turbine (McHenry, 2010)



Figure 2.2: A type of Darrieus (Du, Lee, & Kim, 2009)

So far, many comparisons between various types of Darrieus wind turbine have been carried out. For instance, Jahangir Alam and Iqbal (2009) have worked on performance comparison between Φ -Type and H-Type Darrieus wind turbines. They studied variations of rotor power coefficient and rotor power with respect to rotor tip speed ratio. Their research was indicative of a quick self-starting behavior of the hybrid turbine comparing with the Darrieus type alone. The Savonius wind turbine on the other hand, is vertical axis drag type wind turbines, which are less efficient, compared to horizontal lift-type. However, they are excellent where there is turbulent wind and self-starting is important (Singh, 2008).

However, Altan et al. (2008) in an experimental study, stated a 38.5% improvement of the power coefficient by defining the optimum curtain arrangement. Moreover, Fujisawa and Gotoh (1992) and Fujisawa (1996) have numerically studied the flow field in and around the Savonius rotor. They compared the experimental and numerical results of the effect of the overlaps (ratio of overlap distance between two adjacent blades and rotor diameter) on the flow field in and around a Savonius rotor, by measuring the phase-averaged velocity distributions using the particle imaging velocimetry. The measured velocity distributions for a stationary rotor indicate an increase in flow rate through the overlap from the advancing side to the returning side with increase of the overlap ratio.

There exists a combination of the Darrieus and the Savonius, which has better efficiency than the Savonius and higher starting torque than the Darrieus rotor. Gupta et al. (2008) in their study, compared a three-bucket Savonius rotor with a combined three-bucket Savonius–three-bladed Darrieus rotor. They have stated that the power coefficient of the combined Savonius–Darrieus rotor has dropped at increased overlap ratios unlike the case with three-bucket Savonius rotor.

On the other hand, the horizontal-axis approach currently dominates wind turbine applications. The HAWT designs can be considered a matured industry since several papers and experiments have been performed over many years. A horizontal-axis wind turbine consists of a tower and a nacelle that is mounted on the top of a tower. The nacelle contains the generator, gearbox and the rotor. Horizontal wind turbines (HAWT) were first applied in Europe so that wind technology is beholden to English post-mill and Dutch tower-mill (Righter, 1996).

Figure 2.3 shows a novel innovative application of using wind turbine in urban areas proposed by Arizona State University capable of producing 9,600 kWh electricity per year based on vehicle speeds of 70 mph. Figure 2.4 shows another innovative way of applying wind turbine designed by Atkins designs studio, which is under construction in Dubai.



Figure 2.3: Capturing air turbulence generated by vehicles proposed by an Arizona State University student (Abuelsamid, 2010)

Although, there are horizontal axis wind turbines being used in urban areas such as New Bahrain World Trade Center, the VAWT offer more advantages for locations of low wind speed. Orosa et al. (2009b) reported that the VAWT has simpler construction that can respond more quickly to wind direction or velocity alterations, for easier maintenance and lower attachment costs.



Figure 2.4: The Anara Tower in Dubai (Chino, 2008)

2.1.1 Diffuser Augmented Wind Turbine

Applying a duct is one of the efficient ways to overcome the problem of inferior wind speed. The diffuser augmented wind turbine (DAWT) or so called Ducted Wind Turbine (DWT) was believed to be an efficient way for producing power (S.-H. Wang & Chen, 2008b). The fact that it is more advantageous to apply a shroud and diffuser on a wind turbine was first figured out by Lilley and Rainbird (1956). The first book about the ducted wind turbines was written by James and Petersen (1999). However, due to the lack of a comprehensive description for the flow field of a DAWT, diffuser-augmented wind

turbines were not at the center of attention for many years. In addition, because of the rapid improvement of conventional HAWT, even the research about DAWT seems to have disappeared from the scientific research agenda. However, DAWTs are an interesting subject of current research in which several related papers are published every year. For instance, Mertens (2006) published a PhD thesis, where the diffuser was studied as a wind concentrator that buildings may have on urban wind turbines.

The DAWT is simply a horizontal wind turbine surrounded by a trumpet-bell-shaped diffuser as shown below. Figure 2.5 shows a Vortec Diffuser Augmented Turbine that was developed in New Zealand.



Figure 2.5: Vortec 7 project (Gipe, 1998)

Igra (1981) carried out many wind tunnel experiments with different conclusions. From the wind tunnel data obtained by Igra it can be concluded that the DAWT concept is insensitive to direction changes of the wind between $\pm 30^\circ$. He also claimed that the shrouded

wind turbine is superior to any similar horizontal axis wind turbine of the same diameter for the reasons listed below:

- a) Significant reduction in turbine tip losses
- b) Elimination of the effect of tower wake on the turbine
- c) Being able to use the axial flow turbine due to the flow filed inside the shroud

Foreman et al. (1978) stated that the specific power costs (\$/kW) for a realistic DAWT configuration are found to be lower than conventional wind turbines for very large size rotors, above 50 m diameter, and for rotor diameters less than about 20 m. Foreman et al. concluded that the relative advantages of a diffuser-augmented wind turbine will be sensitive to the type of application; that is, the size of unit, the economic value of a broader operating range, and the local wind spectrum. The initial consistent theory of a simple diffuser was developed by De Vries (1980) and was driven by shrouded turbine theory.

Effects of blade number in Diffuser augmented wind turbine

A DAWT includes a converged inlet to accelerate the wind speed and a diverged tail for controlling the outlet pressure. However, there is not adequate information about how to optimize a ducted wind turbine; the effect of the turbine blade on the wind turbine performance was studied by Wang and Chen (2008a). In their paper they used CFD methods to simulate a specific converging-diverging ducted wind turbine performance. They discovered that the stagger angle and blade numbers have a discrete blockage effect and consequently has effect on wind turbine performance. They showed that a lesser number of blades increase the flow speed while larger blade numbers deliver higher torque. In their research they demonstrated that the maximum power coefficient is between these two extremes.

It is known that the number of blades more than three, usually adopted for these ducted wind turbines, gives maximum torque (Wang and Chen, 2008a). However, increasing the number of blades reduces the entering air flow due to its blockage effect. Furthermore, Duquette and Visser (2003) from comparing the simulation and experimental data stated that the ducted wind turbine efficiency reaches to 44% by applying 12 blades. This shows approximately a 30% improvement to the multi-blades wind turbine efficiency upon Johnson's Study. In addition, pressure distribution between ducted and conventional wind turbine was numerically simulated by (Bet & Grassmann, 2003). Their result also shows an increment of a factor of 2 in wind power.

2.1.2 Climate Effects

Wind power as an important energy source is limited to climate condition. Much research has been carried out in order to investigate the climate impacts on wind turbines. Moist air density and low wind speed are known factors, which increase the possibility of wind power conversion. Orosa et al. (2009a) for instance, has tested wind turbine concentrators to overcome low wind speed in the north of Spain where in the summer there is high humid and low wind speed weather. They considered that moist air is a way to increase wind power conversion. Moreover, in their research, it is reported that for such climate conditions VAWT's are preferred over HAWT due to their simpler construction, which offer quick response to wind speed direction. Breslow and Sailor (2002) have studied the effects climate change on wind speed and consequently its impact on the wind turbines. They have stated that climate change is an important issue for the wind power industry.

2.2 Siting wind turbine in urban area

Wind power is not considered a viable energy source in comparison with solar energy where both are applicable. However, as an interesting substitution to oil product

energy, multipurpose designs to generate renewable energy are the effective and attractive innovation in sustainable energy industry. In the nineties we have observed significant developments in designing, installing and analysis of hybrid (wind, solar and diesel) systems (McGowan & Manwell, 1998). So far, different types of hybrid system have been studied such as wind-diesel systems by Bullock and Musgrove (1987) and hybrid wind-solar by Bakos and Tsagas (2002). The combination of solar and wind energies are being more widely studied and used. For instance, in Dhahran, Saudi Arabia which is the largest oil producing country the feasibility of applying wind-solar-diesel has been investigated by Elhadidy (2002). In addition, many researchers have evaluated financial and economic feasibility of hybrid systems. For instance, Nema et al. (2009) concluded that hybrid green energy is not competitive with conventional fossil fuel in terms of efficiency and cost. But the need for having cleaner power and also improvement in green energy technologies convince many for wide spread use of such systems (Tina, Gagliano, & Raiti, 2006). Furthermore, the proposed wind-solar hybrid renewable energy system by Chong (2009) is also a new conceptual and feasible design in this field.

Van Wijk (1991) has valuated different possibilities for wind turbines to be used in urban areas. He categorized the possibilities as below:

- Stand-alone wind turbines
- Retrofitting wind turbines onto existing buildings
- Wind turbines integrated into the architectural design of structures

As it seemed, the stand-alone is the most problematic possibility mainly because wind speed might be too low and unstable due to environmental obstacles. Furthermore, there are other issues to be solved such as visual pollution, safety and so on.

On the other hand adding wind turbines to existing buildings offers better opportunity for application of wind turbines in cities. Indeed, models of horizontal and

vertical turbines are purposely fabricated for installation on top of the buildings or elevated places. Therefore, small-scale turbines are easily viable as a building retrofitted solution (Bahaj & James, 2007).

Finally, the third suggestion easily could be the best solution due to several advantageous leading to a more effective design. These are integrated into buildings design with a result of less visual pollution

Furthermore, a hybrid wind-solar system also could be used in urban area as a more effective way of producing green energy in cities. Several financial studies have been performed to illustrate the benefits of using hybrid wind-solar systems in urban areas. For instance, Eke et al. (2005) reported that the cost of individual photovoltaic and wind systems is higher than the hybrid sustainable system. Furthermore, Wang et al. (2008) have worked on small turbine blade optimization, proposed to be applied in built up areas and the estimation of the annual power output of the studied turbine.

2.3 Guide Vane

There is inadequate research about the structural analysis of the guide vane or wind concentrators particularly, for those, which are proposed to be installed on the top of high-rise buildings. For instance, Kuma et al. (2008) have studied performance of the straight-bladed vertical axis turbine with a directed guide vane. They stated that directed guide vane and the power coefficient of the proposed wind turbine was approximately 1.2 times higher than that of the original wind turbine, which has no guide vane. Takao et al. (2009) has experimentally investigated the effects of guide vane geometry on power and torque coefficient. Indeed, the concept behind the use of a guide vane is to obtain a higher energy density at the rotor than that in a free flow. This enables us to:

- Produce enhanced power with a defined turbine rotor diameter
- Generate increased power from a defined area of the fluid stream

2.4 Structural Analysis

Interests in investigating the structural behaviors of wind turbine blades have increased in the nineties when there were not adequate tools to design, analyze and develop wind turbines. Most of the research carried out to optimize turbine blade stability and strength used numerical methods, especially Finite Element Method. For instance, El Chazly (1993) used the finite element to inspect the static and dynamic behavior of various blades and different wind speeds. He has analyzed constant chord, tapered and twisted blades and concluded that maximum stresses occurred at the root of the blades for all configurations in the span wise direction. He has stated that tapered blades have the advantage of cutting material weight and reducing the stresses obtained, whereas the twisting of the blade has the benefit of giving more stiffness. In addition, Finite Element has been applied to analyze stress and to optimize composite blade strength (Bechly & Clausen, 1997). Also, the fatigue model and extreme response calculations which take into account both the periodic and the random stress responses were performed and results were compared with the available measured data (Madsen & Frandsen, 1984). Furthermore, study of wind turbine failure has been performed to prevent and learn from the previous disasters. Chou and Tu (2011) investigated the effects of the September 2008, typhoon Jangmi in Taiwan on a collapsed wind turbine tower located on the shore of Taichung Harbor.

Toft and Sorensen (2011) studied a reliability-based design approach for the wind turbine blades. They performed the numerical studies, the reliability of a wind turbine blade based on the single failure mode in both ultimate and fatigue limit states. In the ultimate

and fatigue limit state, the reliability was estimated by taking the information from adequate number of tests.

2.5 Numerical Studies

As a preliminary study Bechly and Clausen (1997) used the 4-node orthotropic thin shell elements and 8-node three-dimensional brick elements in order to simulate the nonlinearity of the rotating aerodynamically-loaded blade of a wind turbine with 400 rpm rotating speed. They have achieved a good agreement between the software predicted results and the experimental tests. Hansen et al. (2000) simulated a DAWT with CFD method and showed that the Betz limit can be exceeded with the ratio corresponding to the relative increase in mass flow through the rotor. Hu and Cheng (2008) conducted an experimentally and numerically research in order to optimize the conventional ducted wind turbine. Combined with optimization process and CAD, they have introduced, manufactured and tested a brand new ducted wind turbine and the results demonstrated significant improvement over conventional turbines. To determine the most appropriate method for flow simulation, the computations for a Savonius type wind turbine are carried out by Dobrev and Massouh (2011) in the following conditions: 2D and 3D flow with $k-\omega$ turbulence model and also 3D flow with DES- $k-\omega$ model. The analysis of obtained rotor power shows that the results of 2D, $k-\omega$ modeling are quite higher than experiments. However, the results of the 3D, $k-\omega$ modeling were quite lower than experiments. Rahimi & Parniani (2009) studied the dynamic behavior including modal and sensitivity analysis eigenvalue tracking, and using it to characterize the instability mode. They verified the time domain simulations results by theoretical studies and stated that the instability occurs due to the mechanical dynamics and it is closely related to increasing generator slip. By employing 3D finite element modeling, Shokrieh and Rafiee (2006) performed the static

analysis for 4 to 25 m/s wind speed to define the critical zone where fatigue failure begins. Experimental and numerical investigations were performed for flow fields of a small wind turbine with a flanged diffuser (Abe et al., 2005) and found agreement between their CFD simulation and the experimental results. It has been stated by Abe et al. that when the performance was normalized by the local mean velocity just behind the turbine blades, both the bare and diffuser-shrouded wind turbines returned almost the same peak performance. Ghasemnejad et al. (2011) used ANSYS software to conduct an experimental and numerical study of buckling and post-buckling failure due to low velocity impacts, in multi-delaminated composite beams which are typically used in wind turbine blade structures. Ghasemnejad et al. used SOLID 46 layered elements with six degree of freedom to predict the critical buckling load and obtained the similar delamination opening according to the relevant experimental results.

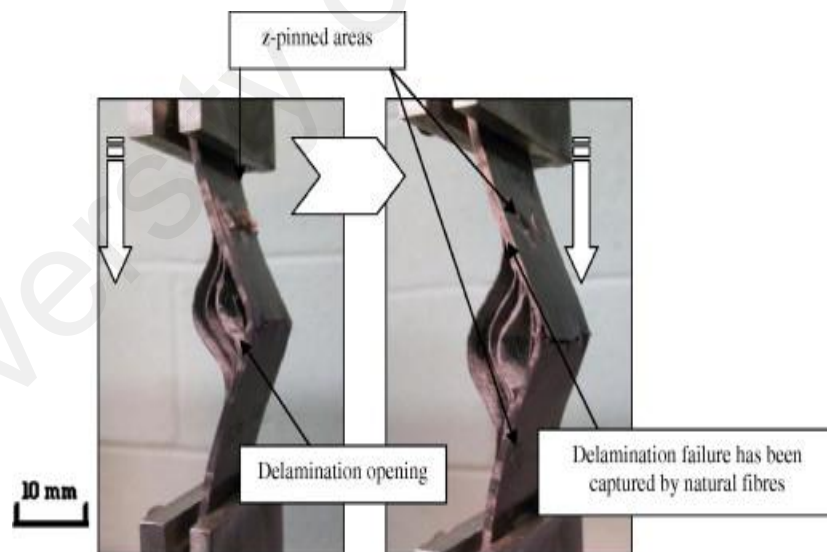


Figure 2.6: Stages of buckling and post-buckling process in laminate design (Ghasemnejad, et al., 2011)

Habali and Saleh (2000) applied the tetrahedron element of four nodes with three degrees of freedom in order to optimize rotor and the blade of a small mixed airfoil wind. Their comparison of the theoretical results and that of the FEM solution was satisfactory

with an acceptable error. Colaciti et al. (2007) indicated that using turbulence models such as Reynolds stress (BSL); the $k-\varepsilon$, the RNG $k-\varepsilon$; and the shear stress transport (SST) $k-\omega$ turbulence models for studying radial diffuser, depends on a compromise between the quality of the results, the number of required simulations, the geometrical and computational characteristics of the simulation. In addition, they stated the poor influence exerted over the flow by the type of boundary conditions applied at the lateral walls. Einberg et al. (2005) selected the standard $k-\varepsilon$ model in order to model turbulence because it represents the best-known model utilized and validated for air diffuser performance. They compared the CFD results with data from laboratory measurements. Their results showed that CFD simulation with a standard $k-\varepsilon$ model accurately predicted non-isothermal airflow around the diffuser. El Kasmi and Masson (2008) developed an extended $k-\varepsilon$ in order to investigate turbulent flow through horizontal wind turbines and compared it to the standard $k-\varepsilon$ results obtained by Crespo (1999).

2.6 Material studies

Blades of horizontal axis are mostly made of composite materials. Composite materials satisfy complex design constraints such as lower weight and proper stiffness, while providing good resistance to the static and fatigue loading. Here, some factors that expose wind turbine blades to the fatigue phenomena are noted (Spera, 1994):

1. Long and flexible structures
2. Vibrations in its resonant mode
3. Randomness in the load spectra due to the nature of the wind
4. Continuous operation under different conditions
5. Low maintenance during lifetime

Noda and Flay (1999) analyzed the fatigue damage occurring at the blade-root of a typical three-bladed Danish-type turbine. Two types of materials, SB-Combi (a glass reinforced polypropylene) and Khaya Ivorensis (a wood epoxy laminate), which are the two most commonly used materials in blade construction today were used and it was concluded that wind shear had a small effect on the blade-root fatigue damage and Stiff blades (i.e. blades with an increased natural frequency) were found to experience increased blade-root fatigue resulting directly from the increased number of load cycles induced by the wind.

A structural design procedure of a medium scale E-glass/epoxy composite wind turbine blade was proposed by Kong et al. (2004). Their procedure, included aerodynamic design, structural design and analysis, fatigue life estimation from the random load spectrum and modal analysis, using FEM for the structural analysis of the proposed design. It was stated that the predicted blade tip deflection and first flap-natural frequency agreed well with the corresponding measured values within 4% error. Habali and Saleh (2000) tested the Glass Fiber Reinforced Plastic (GFRP) rotor blade by installing it on a 15 kW grid-connected-pitch-controlled machine. It was stated that the blade could withstand loads ten times the normal working thrust, with 41.2% measured average power coefficient obtained by the field performance test.

CHAPTER 3

FUNDAMENTAL OF MODELING AND SIMULATION

3.1 Basic Definitions

The purpose of this research is to inspect the structural design of the guide vane to be mounted on high structures. In order to analyze the structural design of the guide vane the following will be taken:

- Computational fluid dynamics
- Finite element method

To calculate the structural stresses and strains, collected wind data will be analyzed and interpreted. Hence, long period wind data from the meteorological station near to the candidate site should be applied. This data must then be carefully analyzed to define the wind profile at the potential site. This wind profile will be used later to investigate the structural behavior of the PAGV.

In order to increase safety and prevent any unexpected failure in structural design a maximum wind speed of 60 m/s will be taken into account (British Standards 6399: part 2). In this study, the mean wind speed and other necessary properties are obtainable for a fixed period of time.

Movement of large masses of air creates one of the main free energy resources known as wind energy. Blades of wind turbines receive kinetic energy of the wind and transform it into different forms of energy such as mechanical and electrical.

The method of inspecting turbine blades is similar to airfoil study. The pressure difference between the upper and lower surfaces of the turbine blade will give a resultant

force, FR. The component of FR perpendicular to the direction of the undisturbed flow is called the lift force, L. The force in the direction of the undisturbed flow is called the drag force; D. Figure 3.1 shows the details.

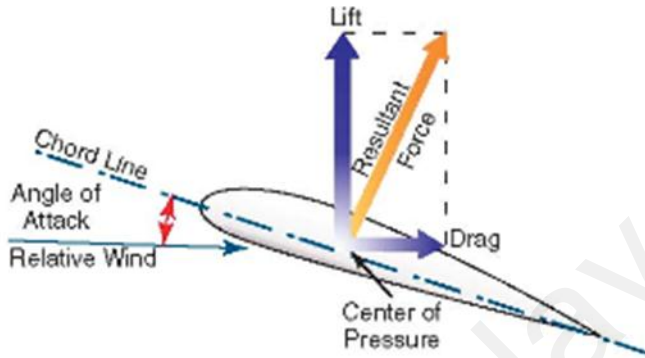


Figure 3.1: The airfoil with velocity of V_∞ meets airflow at shown angle of attack (Federal aviation administration, 2009)

The lift force is given by:

$$L = \frac{1}{2} C_L \rho A V_I^2 \quad (1)$$

And the drag force by:

$$D = \frac{1}{2} C_D \rho A V_I^2 \quad (2)$$

C_L and C_D are dependent on the angle of attack α , which is an angle between the undisturbed wind direction and the chord of the airfoil (shown in Figure 3.1). Both coefficients are affected by the Reynolds number, which is given by:

$$Re = \rho VL / \mu \quad (3)$$

The efficiency of wind energy transformation mainly depends on the turbine system efficiency. In order to optimize the blade shape of a turbine, Lift and Drag forces must be thoroughly investigated. More efficiency will be obtainable for the wind turbine by using ducts to guide the wind and increase the wind speed.

3.1.1 Bernoulli's Principle

The relationship between velocity and pressure exerted by a moving fluid is defined by Bernoulli's principle. Based on Bernoulli's principle an increase in the speed of the fluid simultaneously occurs with a decrease in pressure or a decrease in the fluid's gravitational potential energy. The Bernoulli equation in its original form is valid for incompressible fluids. The Bernoulli equation for incompressible fluid is:

$$P/\rho + (V^2)/2 + gz = \text{constant} \quad (4)$$

Bernoulli's equation is only applicable to incompressible fluids and compressible fluids at very low speeds. It is possible to use the fundamental principles of physics to develop similar equations applicable to compressible fluids. There exist numerous equations each tailored for a particular application, which are all derived from Bernoulli's law.

3.1.2 Venturi Effect

The Venturi effect is an example of Bernoulli's principle for the case of incompressible flow through a tube with a constriction in it. The fluid velocity increases through the constriction to satisfy the equation of continuity, while its pressure decreases due to the conservation of energy; a drop in pressure or a pressure gradient force supplies the gain in kinetic energy. The pressure difference is useful in many applications. Since the pressure difference can be measured directly, the obtained pressure difference can be related to an unknown velocity; which will be calculated by Bernoulli's equation and continuity equation. The venturi effect is used to obtain increased wind speed in PAGV design due to its difference in area.

3.2 Computational Fluid Dynamics (CFD)

Today, applying numerical methods to solve engineering problems seems inevitable to solve complex engineering problems. Methods such as CFD are used more and more due to rapid growing computer technologies, which solve mathematic problems faster and more reliable. Applying numerical solution to fluid mechanic has made a lot of unsolvable problems and expensive experimental tests to be analyzed and simulated. However, for more complicated cases, experimental practices need to be implemented in order to avoid inevitable errors such as iterations errors. In fact, governing equations for a fluid will be driven from the fundamental laws of mechanics. The conservation of mass, the conservation of momentum and conservation of energy equation form a set of coupled, nonlinear partial differential equations. To most of engineering problems, there is low possibility to solve these equations analytically.

On the other hand, it is possible to find approximate computer-based solutions to the governing equations in order to solve engineering problems. Generally, the aim of CFD is to simplify and replace continues problem domain to discrete domains by using grid. This illustrates the importance of Computational Fluid Dynamics in engineering. It can be shown by an example comparing continues pressure and discrete pressure. Below equation shows continues pressure in one dimension domain. The concept of continuous and discrete was shown in Figure 3.2.

$$p = p(x) \quad 0 < x < 1$$

While for discrete domain it is

$$p_i = p(x_i) \quad i = 1, 2, \dots, N$$

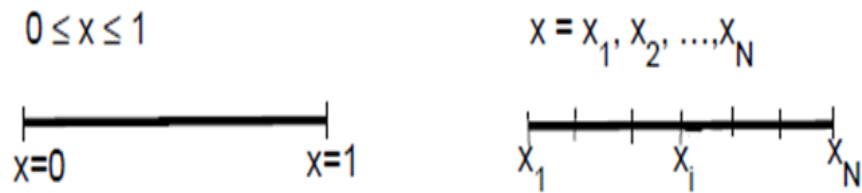


Figure 3.2: Continues domain and discrete domain (x_i : Grid point)

In a CFD solution, one will directly solve for the relevant flow variables only at the grid points. The other location values will be defined by interpolation of the values at the grid points.

To numerically solve fluid mechanical problems, defining initial and boundary condition is required. In fact, to define boundary conditions in mathematics is a basic principle. However, in the numerical method, to define physical boundary conditions is needed to solve problems. The governing partial differential equations and boundary conditions in exact solution are defined in terms of continuous variables such as pressure, velocity and so on. These can be approximated in the discrete domain in terms of the discrete variables. The discrete system is a large set of coupled, algebraic equations in the discrete variables. Setting up the discrete system and solving it involves a large number of repetitive calculations. The fact of encountering huge calculation has restricted numerical calculation to digital computers. Fluent is one of the useful computational fluid mechanic software for analyzing fluids flow.

3.2.1 Discretization Methods

Basically, there exist two methods of discretization. The first and simplest is called finite-difference method. By applying the fundamentals of CFD to the one-dimensional equation, the finite-difference method will be illustrated.

$$u^m + \frac{du}{dx} = 0 \leq x \leq 1 \quad u(0) = 1 \quad (5)$$

For the linear conditions, the above equation will appear in the discrete domain as:

$$\left(\frac{du}{dx}\right)_i + ui = 0 \quad (6)$$

U_{i-1} will be expanded in Taylor's series in order to get an expression for $\frac{du}{dx}$ in terms of u at the grid points.

$$U_{i-1} = u_i - \Delta x \left(\frac{du}{dx}\right)_i + O(\Delta x^2) \quad (7)$$

After rearrangement:

$$\left(\frac{du}{dx}\right)_i = \frac{U_i - U_{i-1}}{\Delta x} + O(\Delta x) \quad (8)$$

$O(\Delta x)$ is called the truncation error, which is due to the neglected terms in the Taylor's series so that the discrete equation is defined as the first order accurate. By applying equation (3) in equation (2), we will have:

$$\frac{U_i - U_{i-1}}{\Delta x} + U_i = 0 \quad (9)$$

The finite-difference method derives the discrete equation using Taylor's series expansions while higher order terms are neglected. Although, this method is not used by the most software, it is important to comprehend the concept of different discretization methods.

The second discretization method is called finite-volume method, which is used by CFD software such as ANSYS Fluent. In the method of finite-volume, the integral form of the conservation equations will be applied to the control volume, which is defined by a cell.

So, the discrete equations of the cell are obtained. The integral form of the continuity equation for the steady, incompressible flow is:

$$\int_S V \cdot n \, ds = 0 \quad (10)$$

The equation above is physically understood as the net volume flow into the control volume of zero. Figure 3.3 shows a rectangular cell used to write the velocity vector. The velocity vector is written as:

$$\vec{V}_i = \vec{u}_i i + \vec{v}_j j$$

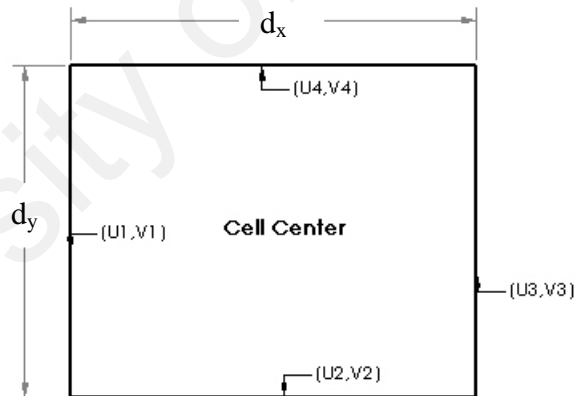


Figure 3.3: A rectangular cell

Applying the continuity equation to the cell control volume gives:

$$-u_1 \Delta y - v_2 \Delta x + u_3 \Delta y + v_4 \Delta x = 0$$

This is the discrete form of the cell continuity equation. Conservation of momentum and energy for the cell are obtained using the same method. The partial differential equation is valid at all points in the domain which it is considered as infinitesimal volumes.

Anticipating that infinitesimal discrete volumes are unaffordable and would have to be inflated to a finite size. The conservative form for a finite volume δV bounded by a surface δS would be

$$\frac{d}{dt} \left(\int_{\partial v} T dV \right) + \int_{\partial s} \vec{n} \cdot \vec{u} T dV = \int_{\partial s} \vec{n} \alpha \nabla T dV \quad (\text{M. Iskandarani, 2002})$$

Here \vec{n} is the outward unit normal to the surface δS . It was assumed that volume δV to be fixed in space so the order of integration in space and differentiation in time is interchangeable. The interpretation of the first integral on the left hand side simply is the time rate of change of the T budget inside volume δV . The Gauss-divergence theorem is used to change the volume integrals of the flux and diffusion divergence into surface integrals. The surface integral on the left hand side accounts for the advective flux carrying T in and out of the volume δV across the surface δS . The surface integral on the right hand side accounts for the diffusive transport of T across δS . Since abovementioned integrals are exact and no approximation was necessary in their derivation; in a numerical model, the approximation will be introduced by the temporal integration of the equations, and the need to calculate the fluxes in space and time. The traditional finite volume method takes equation below (using the average T in ∂v) as its starting point.

$$\partial v \frac{d\bar{T}}{dt} + \int_{\partial s} \vec{n} \cdot \vec{u} T dV = \int_{\partial s} \vec{n} \alpha \nabla T dV$$

The domain is first divided into computational cells δV_j where the cell average of the function is known. The advection and diffusion fluxes are calculated in following steps:

a) Function reconstruction:

The advective fluxes require the calculation of the function values at cell edges, while the diffusive fluxes require the calculation of the function derivative at cell edges. The latter are obtained from approximating the function T with a polynomial whose coefficients are determined by the need to recover the cell averages over a number of cells.

b) Evaluation of the integrals: The integrals are usually evaluated numerically using Gauss type quadrature. The approximation function ϕ_n generally determine the number of quadrature points so that the quadrature is exact for polynomials of degree P . No error is then incurred during the spatial integration.

The final source of error originates from the temporal integration whereby the fluxes are used to advance the solution in time using a time marching procedure a la Forward Euler, one of the Runge Kutta methods, or the Adams-Bashforth class of methods. The time integration cannot be chosen independently of the spatial approximation however, it is usually constrained by stability considerations.

3.2.2 Solution Convergence

A discrete system is a bunch of simultaneous equations formed from the discrete equation. Truncation error in discrete system is reduced as the number of it is increased.

Thus, there will be agreement between the exact and the numerical solution. When, the CFD results obtained on different points agree to within a specified tolerance level, they are called convergence solution.

3.2.3 Nonlinearity

High nonlinearity is an obstacle to obtain an accurate numerical solution for complicated problems. Existence of nonlinear equations, chemical reactions and turbulence are main factors of nonlinearity. However, to confront nonlinear equations, the chosen strategy is to linearize the equations about a guess value. The method is to be iterated until it converges to a specified tolerance level. As well, iteration is a factor of CFD not only for nonlinearity but also for linearity because it effectively reduces the time of calculations. At

last, the iteration is performed until the difference between the solution and guess is small enough.

3.2.4 Turbulence Models

Varying the velocity, pressure and so on can cause non-linearity, which builds turbulent flow. Turbulence models are applied to predict the effects of turbulence on the flows without directly solving the non-linear equations. So far, many computational models for turbulence with varying levels of complexity have been developed. These can be generally categorized into four methods (ANSYS help system, Release 13.0):

- Direct Numerical Simulation (DSN)
- Large Eddy Simulation (LES)
- Reynolds-averaged Navier-Stokes (RANS)
- Detached eddy simulations and other hybrid models

Some of these models are applied to a wide range of flows while some are used specifically. These models are all developed based on Navier–Stokes equations.

DNS as a method of computational fluid dynamics solves the Navier-Stokes equations numerically without any turbulence modeling and the spatial and temporal scales of the turbulence are solved. All the spatial scales of the turbulence associated with the motion containing most of the kinetic energy are analyzed in the computational mesh.

DNS is a useful research tool but is considered relatively expensive, even for a case of low Reynolds numbers. Consequently, for more common Reynolds numbers in industrial application, DNS method needs super computers to simulate problems. However, DNS a desirable method to enhance the understanding of the turbulence physics. Indeed, the input data for other models such as LES and RANS are obtained from DNS simulation. In

addition, to avoid the cost of experimental tests the results of other turbulence model can be evaluated by those obtained using DNS.

Large eddy simulation (LES) is a less complex numerical technique applied to solve the partial differential equations of turbulent fluid flow. Based on Kolmogorov's (1941) famous theory of self-similarity, large eddies of flow are dependent on flow geometry, while smaller eddies are self-similar and have a universal characteristic. Therefore, to obtain a solution for only large eddies seems practical. Furthermore, effects of the smaller and more universal eddies are modeled on the larger ones. Thus, sub-grid scales (SGS) modeling will be applied to present the effects of small-scale fluid motion such as small eddies, swirls and vortices, in the equations governing large-scale motion. Indeed, in LES, only the large scale motions of the flow are resolved by the computer while effects of the smaller scales are modeled by SGS. Hence, in practical problems, obviously LES requires less computational time and effort in comparison with DNS. However, the computation often exceeds the capacity of most computers for simulating flows in the vicinity of walls. In order to remove this problem, empirically based models such as RANS replace LES in the wall region.

The main advantage of LES compared to some less accurate but computationally cheaper approaches is the more accurate and detailed result. This can be significant in particular where the simulation involves chemical reactions like the investigation of combustion engines where the accurate concentration of chemical species is inevitable to start a reaction. However, it is possible to have localized areas of high concentration where reactions will occur. In addition, LES is strongly recommended where there exists flow separation or acoustic prediction.

RANS is the least accurate approach to turbulence modeling. A group of governing equations are solved to introduce new apparent stresses known as Reynolds stresses.

However, statistically unsteady (or non-stationary) flows can be solved in a similar way, since RANS equations are time-average equations. Therefore, there could be a misconception that RANS equations are not applicable to a time-varying mean flow. Yet, the turbulence model is valid only as long as the time scales of the turbulent motion, containing most of the energy is small enough to compare the time scale of these changes in the mean.

In general, RANS model can be summarized into two approaches:

- Boussinesq hypothesis
- Reynolds stress model (RSM)

The Boussinesq hypothesis uses an algebraic equation for the Reynolds stresses to determine the turbulent viscosity. It is also used to obtain the turbulent kinetic energy and dissipation by solving transport equations dependent upon the problems requirements. The number of transport equations defines the approach of the model. For instance, no transport equation is solved in a Mixing Length model so it is called a Zero Equation.

RSM on the other hand, attempts to introduce several transport equations to all Reynolds stresses. Obviously, this costs more and takes more time as well as CPU effort. In fact, RANS as the most common computational method of solving fluid problems is broadly applied in commercial software such as ANSYS Fluent, ANSYS-CFX and so on.

In a more general view, turbulence models based on the mentioned approaches, based on ANSYS Fluent can be presented as below:

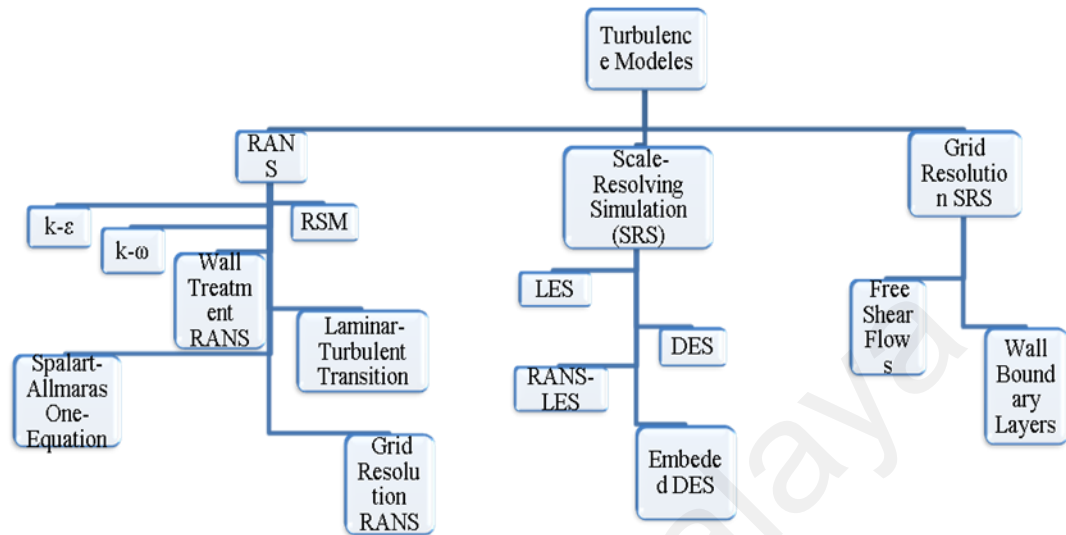


Figure 3.4: Hierarchy of turbulence models in ANSYS Fluent

3.3 k - ε Turbulence Model

k - ε is one of the most common and applicable two transport equations turbulence models. It is the standard multipurpose model, which is recommended for most of industrial simulations. Moreover, it is a robust computational method delivering acceptable results in comparison with computational and experimental tests, which make it a combination of accuracy and powerful abilities. The term, k , stands for the first transport variable which is the turbulent kinetic energy and similarly, ε , is the scale of the turbulence or the kinetic energy dissipation rate. It is the simplest complete models of turbulence in which the solution of two separate transport equations allows the turbulent velocity and length scales to be independently determined. The transport equation for the k was derived from the exact equation while the ε was obtained using physical reasoning and is different to its some mathematical counterpart.

However, after applying this model for several years it's advantageous and weaknesses have been discovered. Modifications in k - ε model can be noted as standard, RNG, and realizable models. The main differences between three k - ε models are listed below.

- The method of calculating turbulent viscosity
- The turbulent Prandtl numbers governing the turbulent diffusion of k and ε
- The generation and destruction terms in the ε equation

The transport equations for the Standard/RNG k - ε Model k - ε are shown here. The kinetic energy and its dissipation in standard k - ε are derived from the following transport equation (ANSYS help system, Release 13.0).

$$\frac{\partial}{\partial t}(\rho k) + \frac{\partial}{\partial x_i}(\rho k u_i) = \frac{\partial}{\partial x_j} \left[\left(\mu + \frac{\mu_t}{\sigma_k} \right) \frac{\partial k}{\partial x_j} \right] + G_k + G_b - \rho \varepsilon - Y_M + S_k \quad (11)$$

$$\frac{\partial}{\partial t}(\rho \varepsilon) + \frac{\partial}{\partial x_i}(\rho \varepsilon u_i) = \frac{\partial}{\partial x_j} \left[\left(\mu + \frac{\mu_t}{\sigma_\varepsilon} \right) \frac{\partial \varepsilon}{\partial x_j} \right] + C_{1\varepsilon} \frac{\varepsilon}{k} (G_k + C_{3\varepsilon} G_b) + C_{2\varepsilon} \rho \frac{\varepsilon^2}{k} + S_\varepsilon \quad (12)$$

Default values of the model constants $C_{1\varepsilon}$, $C_{2\varepsilon}$, C_μ , σ_k , σ_ε are listed below.

$$C_{1\varepsilon} = 1.44 \quad C_{2\varepsilon} = 1.92 \quad C_\mu = 0.09 \quad \sigma_k = 1.00 \quad \sigma_\varepsilon = 1.30$$

In similar way, RNG k - ε model has an almost similar transport equations which are:

$$\frac{\partial}{\partial t}(\rho k) + \frac{\partial}{\partial x_i}(\rho k u_i) = \frac{\partial}{\partial x_j} \left[\mu_{eff} \frac{\partial k}{\partial x_j} \right] + G_k + G_b - \rho \varepsilon - Y_M + S_k \quad (13)$$

$$\frac{\partial}{\partial t}(\rho \varepsilon) + \frac{\partial}{\partial x_i}(\rho \varepsilon u_i) = \frac{\partial}{\partial x_j} \left[\mu_{eff} \frac{\partial \varepsilon}{\partial x_j} \right] + C_{1\varepsilon} \frac{\varepsilon}{k} (G_k + C_{3\varepsilon} G_b) + C_{2\varepsilon} \rho \frac{\varepsilon^2}{k} + S_\varepsilon \quad (14)$$

3.4 Realizable k - ε Model

Realizable k - ε model is a relatively recent development of standard k - ε model which is distinguished due to two new characteristics of, new formulation for the turbulent viscosity and a new transport equation for the dissipation rate derived from the exact

equation of the transport of the mean-square vorticity fluctuation. In fact, realizable means that the model satisfies certain mathematical constraints on the Reynolds stresses, in agreement with the physics of turbulent flows. The transport equation of this model is (ANSYS help system, Release 13.0):

$$\frac{\partial}{\partial t}(\rho k) + \frac{\partial}{\partial x_i}(\rho k u_i) = \frac{\partial}{\partial x_j} \left[\left(\mu + \frac{\mu_t}{\sigma_k} \right) \frac{\partial k}{\partial x_j} \right] + G_k + G_b - \rho \varepsilon - Y_M + S_k \quad (15)$$

$$\frac{\partial}{\partial t}(\rho \varepsilon) + \frac{\partial}{\partial x_i}(\rho \varepsilon u_i) =$$

$$\frac{\partial}{\partial x_j} \left[\left(\mu + \frac{\mu_t}{\sigma_\varepsilon} \right) \frac{\partial \varepsilon}{\partial x_j} \right] + \rho C_{1\varepsilon} S_\varepsilon - \rho C_{2\varepsilon} S_\varepsilon \frac{\varepsilon^2}{k + \sqrt{\nu \varepsilon}} + C_{1\varepsilon} \frac{\nu}{k} C_{3\varepsilon} G_b \quad (16)$$

Where:

$$C_1 = \max\left[0.43, \frac{\nu}{\nu + 5}\right], \quad \nu = S \frac{K}{E} \quad \text{and} \quad S = \sqrt{2 S_{ij} S_{ij}}$$

In fact, $k-\varepsilon$ models can include many different cases however, in ANSYS Fluent, the use of the Realizable $k-\varepsilon$ model is recommended relative to other variants of the $k-\varepsilon$ family.

3.5 Boundary Conditions

In general, ANSYS Fluent software classifies the boundary conditions into four main types:

- Inlet and outlet boundaries (velocity inlet, pressure inlet...)
- Walls boundaries (pressure far field, outflow, axis...)
- Cell boundaries (fluids and solids)
- Inside surfaces (porous jumps, fan, interior an radiator)

Table 3.1 introduces all the categories of boundary conditions used in the Fluent software.

Table 3.1: Boundary conditions in ANSYS Fluent

Category	Zone Types
Faces	Axis, Outflow, Mass flow inlet, Pressure Far-field, Pressure inlet, Pressure outlet, Symmetry, Velocity inlet, wall, Inlet vent, Intake fan, Outlet vent, Exhaust fan
Double-Sided Faces	Fan, Interior, Porous jump, Radiator, Wall
Periodic	Periodic
Cells	Fluid, Solid (porous is a type of fluid cell)

3.6 Finite Element Method

Finite element method (FEM) presents a fast, uncomplicated and reliable way to predict complex structural design behavior based on numerical methods. Finite elements are methods to solve problems by dividing it into small pieces and solving them with an acceptable approximation. Indeed, there are some instances of finite elements in our life as well as in engineering. An understandable example is to calculate the area of a circle by forming internal triangles. So, the area of a circle is approximated to a summation of triangle areas. As a matter of fact, FEM is widely being applied to engineering problems due to its great compatibility with CAD/CAM software.. Hence, current problems for most mechanical, aerospace, automobile and civil engineering is handed over to FEM.

There exist many types of elements, which are used in FE due to the physics of the problems. However, it is important to note that any type of element must satisfy the convergence criteria. In fact, to determine shape functions it is important to select proper element type. Element types are defined based upon their shapes, node numbers, nodal

variables and their interpolation functions. Generally, elements can be classified into three main categories. Figure 3.4 to Figure 3.7 show the one dimensional, two-dimensional and three-dimensional elements:

One-dimensional elements are:



Figure 3.5: Linear, quadratic and cubic one-dimensional element

Two-dimensional elements are:

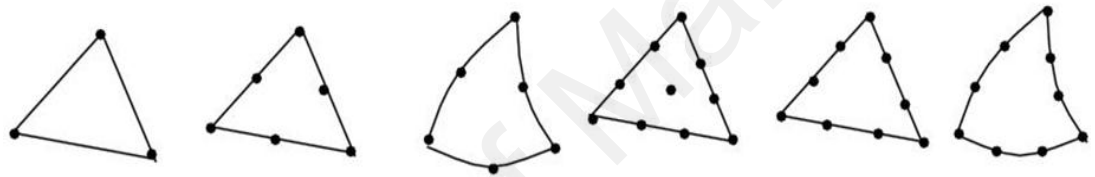


Figure 3.6: Linear triangular, quadratic triangular and cubic triangular; two-dimensional element

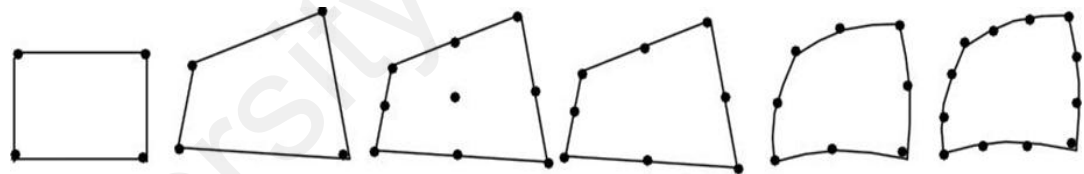


Figure 3.7: Linear rectangular and quadrilateral, quadratic quadrilateral and cubic quadrilateral three-dimensional element

Three-dimensional elements are:

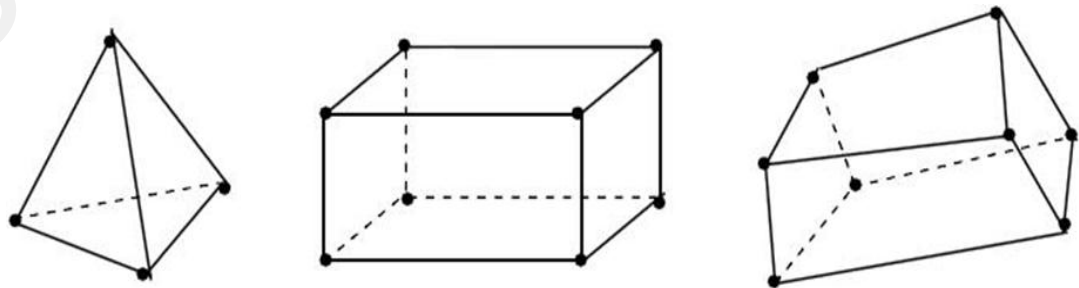


Figure 3.8: Tetrahedron, Right Prism, Hexahedron; three-dimensional element

Today, there a long list of FEM software with uses for single or multipurpose aims. However, the most common FE software are ANSYS, Abaqus and Nastran.

3.7 Failure Theories

There are several commonly accepted failure theories for yielding in a general state of stress. The two most commonly applied are the Maximum Shear Stress Theory (MSST) and the Distortion Energy Theory (DET). The MSST holds that failure (yielding) in a general state of stress occurs when the maximum shear stress as given equals or exceeds the maximum shear stress occurring in a uniaxial tension test at yielding.

The energy DET is based on the strain energy stored in a material under a given state of stress. The theory holds that a uniform tensile or compressive state of stress (hydrostatic stress) does not cause distortion and, hence, does not contribute to yielding. If the principal stresses have been computed, total elastic strain energy is given as (Hutton, 2003):

$$Ue = \frac{1}{2E} [\sigma_1^2 + \sigma_2^2 + \sigma_3^2 + \sigma_1\sigma_2 + \sigma_1\sigma_3 + \sigma_2\sigma_3]V \quad (17)$$

By defining the average stress as:

$$\sigma_{avg} = \frac{\sigma_1 + \sigma_2 + \sigma_3}{3} \quad (18)$$

We will have corresponding strain energy as:

$$U_{hyd} = 3 \frac{\sigma_{avg}^2}{2E} (1 - 2\nu)V \quad (19)$$

The distortion energy in terms of the principal stress components is found to be given by:

$$U_d = \frac{1+3\nu}{2E} V \sqrt{\frac{(\sigma_1 - \sigma_2)^2 + (\sigma_1 - \sigma_3)^2 + (\sigma_2 - \sigma_3)^2}{2}} \quad (20)$$

The DET states that failure (yielding) occurs in a general state of stress when the distortion energy per unit volume equals or exceeds the distortion energy per unit volume occurring in a uniaxial tension test at yielding.

Where from the yielding in a tensile test, the distortion energy is given by:

$$U_d = \frac{1+\nu}{3E} S_y^2 V \quad (20)$$

From the last two equations we will have the failure (yielding) criterion for the DET as following:

$$\sqrt{\frac{(\sigma_1 - \sigma_2)^2 + (\sigma_1 - \sigma_3)^2 + (\sigma_2 - \sigma_3)^2}{2}} \geq S_y \quad (21)$$

The DET as described in above equation leads to the concept of an equivalent stress (known historically as the Von Mises stress) defined as:

$$\sigma_e = \sqrt{\frac{(\sigma_1 - \sigma_2)^2 + (\sigma_1 - \sigma_3)^2 + (\sigma_2 - \sigma_3)^2}{2}} \quad (22)$$

and failure (yielding) can then be equivalently defined as:

$$\sigma_e \geq S_y$$

Nevertheless, every finite element software package not only computes strain and stress components in the global and element coordinate systems but also principal stresses and the equivalent (Von Mises) stress for every element.

The DET can be shown to be equivalent to another elastic failure theory, known as the octahedral shear stress theory (OSST). For all practical purposes, the OSST holds that yielding occurs when the maximum shear stress exceeds $0.577S_y$. In comparison to the MSST, the OSST gives the material more “credit” for strength in shear.

3.8 Failure Theories

Despite the fact that there exist varieties of materials, engineering structures are formed from relatively defined materials. In fact, many structures are designed to tolerate only elastic loads. Isotropic and homogeneous materials such as steels, irons and aluminums are more often used to fabricate common structures. Although there are composite and polymeric materials, their complex behavior and relatively higher costs, persuade engineers to not use them in conventional structures. Figure 3.8 shows the stress-strain diagram for three different materials, assisting to have a general view of selecting material.

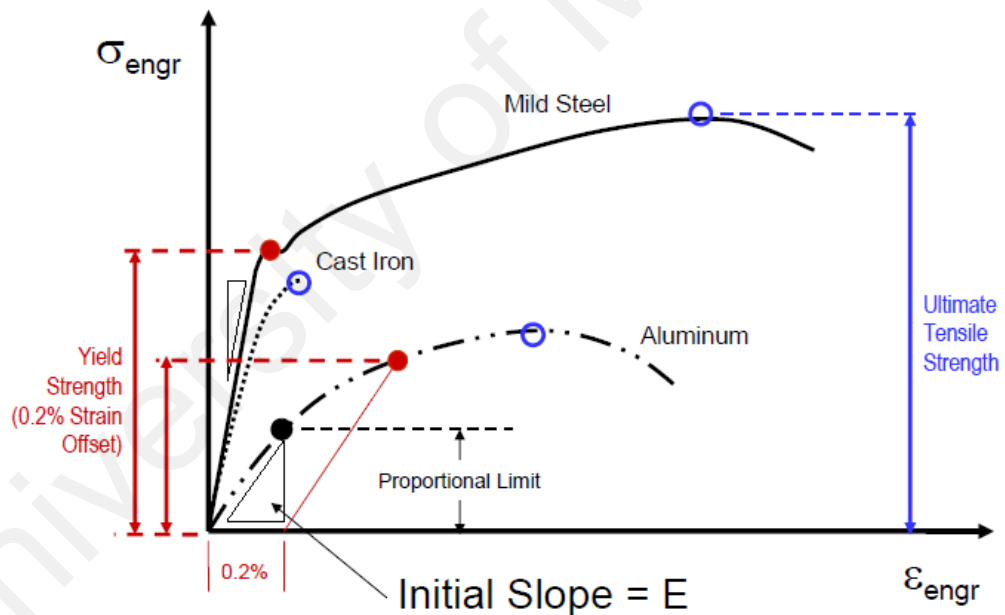


Figure 3.9: Stress, strain diagram of different materials (ASM, 2002)

As it is shown in the diagram steel, is essentially at the center of attention due to its high material and mechanical properties. Table 3.2 presents a list of the most common materials used in structures.

Table 3.2: General properties of common structure material (Hibbeler, 2011)

Material	ρ Kg/m ³	E GPa	G GPa	σ_y MPa	σ_u MPa	ϵ
Aluminum	2768	73	27	276	414	0.35
Aluminum 2024						
Aluminum 6061						
Titanium	4429	120	44	924	924	0.36
Steel	7832	200	27.6	1170	1240	11.9
AISI 4340						
AMS 6520						
Stainless						
300 M						
Plastic	1450	131	76	...	0.34
Kevlar 49						
30 % Glass						
Wood	470	13.1	...	65	...	0.29
Spruce						
Fir						
	360	9.65	...	47	55	0.31

CHAPTER 4

SIMULATION OF THE PAGV

4.1 Research Background

The PAGV is mounted at high-rise buildings or structures where, it can harness higher wind speed. Figure 1.1 shows general arrangement of the system. However, in reality, it can be of any shape dependent upon the building architecture profile. The wind turbine, [A], is located in the middle of the system, surrounded by the PAGV which was designed to enhance wind power extraction by replacing the free stream from wind through multiple channels of the speed-increased and directional-controlled air-stream. The PAGV consists of an upper wall duct, [D], a lower wall duct, [E], and guide vanes, [B]. The PAGV is designed to be fixed or yaw-able with the help of a rudder, [C], or pressure sensors and servomotor, to face the on-coming wind stream. The PAGV collects radial wind stream

from a larger area and creates a venturi effect to guide and increase the wind speed before it enters the wind turbine. The wind turbine and the PAGV have a common rotating axis. The center drive shaft of the VAWT is coupled with the generator, [I], through the power transmission shaft and mechanical drive system, [H], such as a gear system. The PAGV consists of vanes of variable sizes or shapes having constant or varying thickness, in which they are positioned surrounding the turbine. The upper and lower wall ducts are inclined at an angle, θ , from the horizontal plane. The exterior surface of the upper wall of the PAGV provides the base for placement of solar panels (solar photovoltaic and/or solar thermal panel), or solar concentrator system. The multi-sector arrangement of solar panels, on top of the upper wall duct, is inclined to harness solar energy from multiple angles of the sun. At the same time, the multi-sector arrangement of these inclined solar panels also form the flow path for guiding the rainwater towards the center of the system. The rainwater then flows through the rainwater passage in the middle of the system and is stored in the water storage compartment at the bottom.

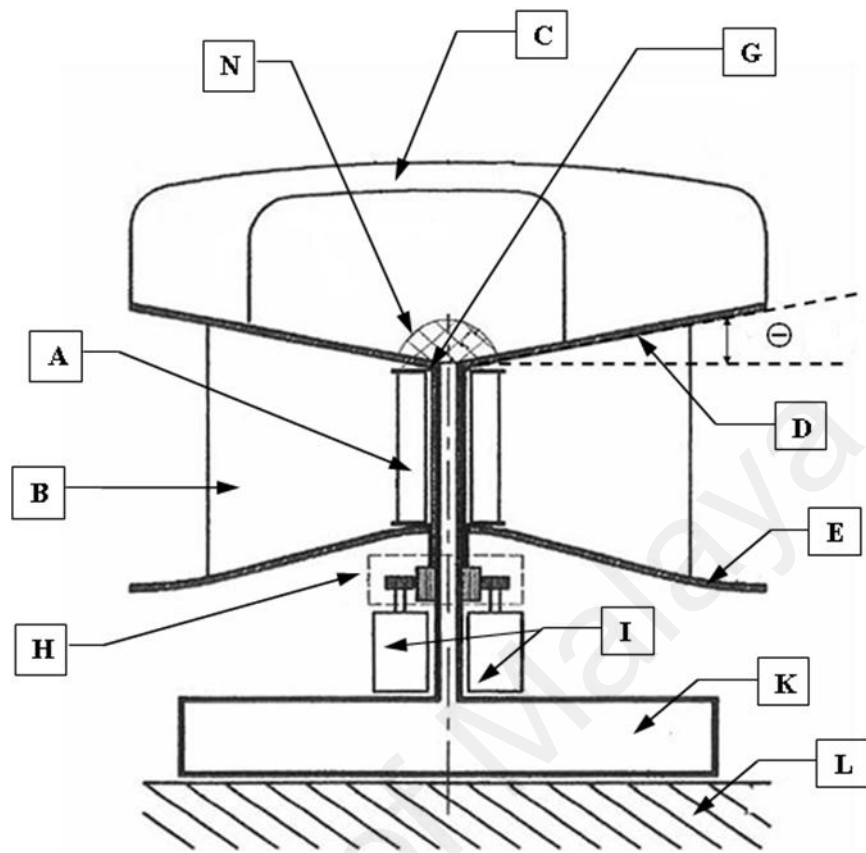


Figure 4.1: Sectional view of the wind-solar hybrid renewable energy generation system with rainwater collection feature (Chong et al., 2009)

Nevertheless, to install the PAGV on the top of high-rise buildings, different environmental condition must be considered. In particular, unexpected weather conditions such as storms, illustrate the significance of the structural design of the PAGV. Only with a reliable structural analysis can the PAGV be safely applied on top of high-rise buildings. Thus, the requirement of structural design analysis seems to be unavoidable.

4.2 Initial Design

The patented PAGV was designed by Chong et al. (2009) to guide and direct the wind through the select turbine based on the Venturi effect. The PAGV can be mounted on high rise buildings in urban or remote areas. The process of the PAGV design introduced

by Chong et al. (2009) has been computer aided. Thus, to get the best angle of attack on the vanes of PAGV, and also the most efficient combination of vanes, they applied Gambit and Fluent in order to analyze the PAGV. Besides, they have performed experimental tests in order to ensure that the computer obtained results are justified. Figure 4.2 shows the proposed PAGV by Chong et al. (2009) and Figure 4.3 shows the design together with the additional supports.

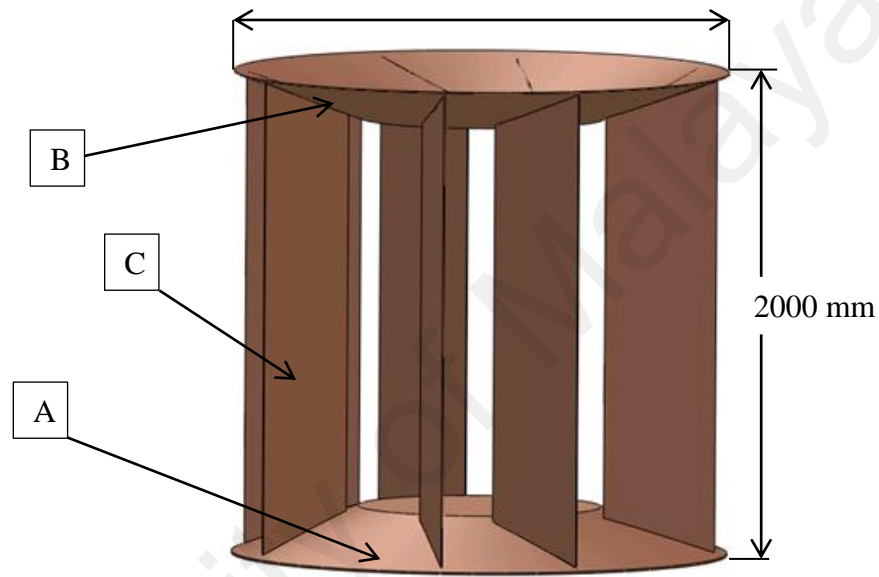


Figure 4.2: The initial PAGV design

The proposed PAGV is consisted of a lower wall duct, [A], an upper wall duct, [B], and guide vanes, [C]. A supporting arm, [D], supports each guide vane to increase the stability of the PAGV.

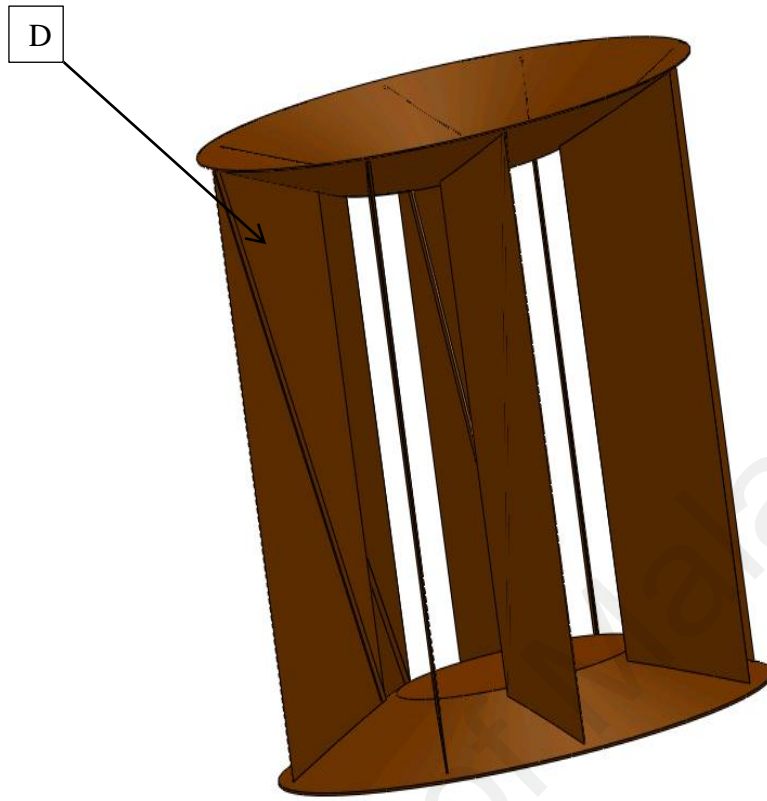


Figure 4.3: The initial PAGV design together with the supports

In accordance with the space availability and select turbine the, dimension of PAGV is defined. The primary height and outer diameter of the PAGV are respectively 2200 mm and 2040 mm. On account of the limited ability of normal computers which disallow us to analyze relatively large volumes, the primary dimensions will be scaled to half of the initial dimensions. The PAGV mounted on a provided T-shape support (Figure 4.6). Figure 4.4 shows the top view of the scaled PAGV designed.

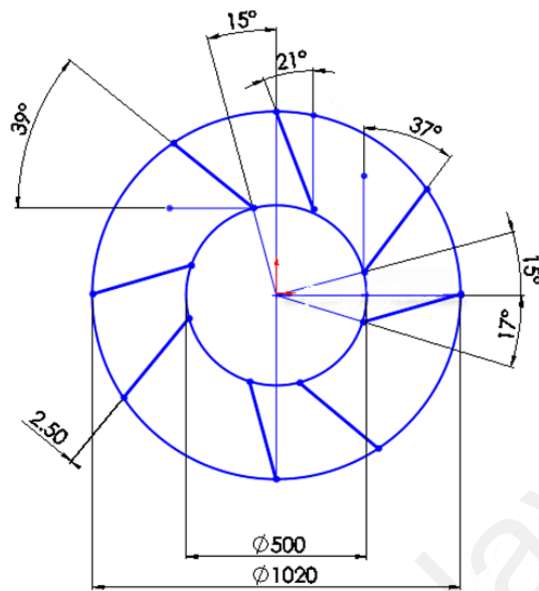


Figure 4.4: The PAGV-Sectional view

On the other hand, because PAGV is mounted on the top of buildings; the total weight of it will be a matter of concern. Thus, to achieve safest, most efficient design while maintaining the initial shape, properly designed supports and material choice are significant

4.3 Material Properties

To define a proper material for a particular design is the one of first and the most significant parts of any structural design. In this section, the process of defining material for the proposed PAGV will be presented.

In order to select the best PAGV material, maintaining the whole weight of the structure as low as possible is the pivotal goal. Besides, the effects of tropical weather conditions must be thoroughly considered. Moreover, ductile materials are better than brittle ones, because peak stresses at the root of the crack are reduced by local plastic deformation. Highly loaded guide vanes, diffusers or shafts should therefore have a minimum ultimate elongation, $A > 15\%$ (preferably $A > 25\%$). Hence, for surfaces directly exposed to the outside weather, which consist mostly of the PAGV parts, alloy steel is

suggested due to its acceptable yield and ultimate stress. Besides, it is resistant to erosion and corrosion. The safety factor for any material can be calculated as:

$$\text{Safety factor} = \frac{\sigma_{max}}{\sigma_y}$$

Where σ_{max} is the maximum stress and σ_y is the yield stress of the material.

However, to simplify the simulation of the PAGV was assumed to be at uniform material which, were perfectly connected.

4.4 Support Configuration

In order to preserve the initial weight of the PAGV to the very possible extent, guide vanes are made from low thickness alloy steel supported by rectangular steel bars. The top and bottom of the PAGV is designed to be made from alloy steel relatively resistant to erosion and corrosion. In such a way, the guide vanes of the PAGV will be resistant to humid and dusty weather. Moreover, the whole structure will have the least possible added weight, which increases the feasibility of applying PAGV on top of buildings or structures. Figure 4.5 shows the section view of a guide vanes supported by supporting arm.

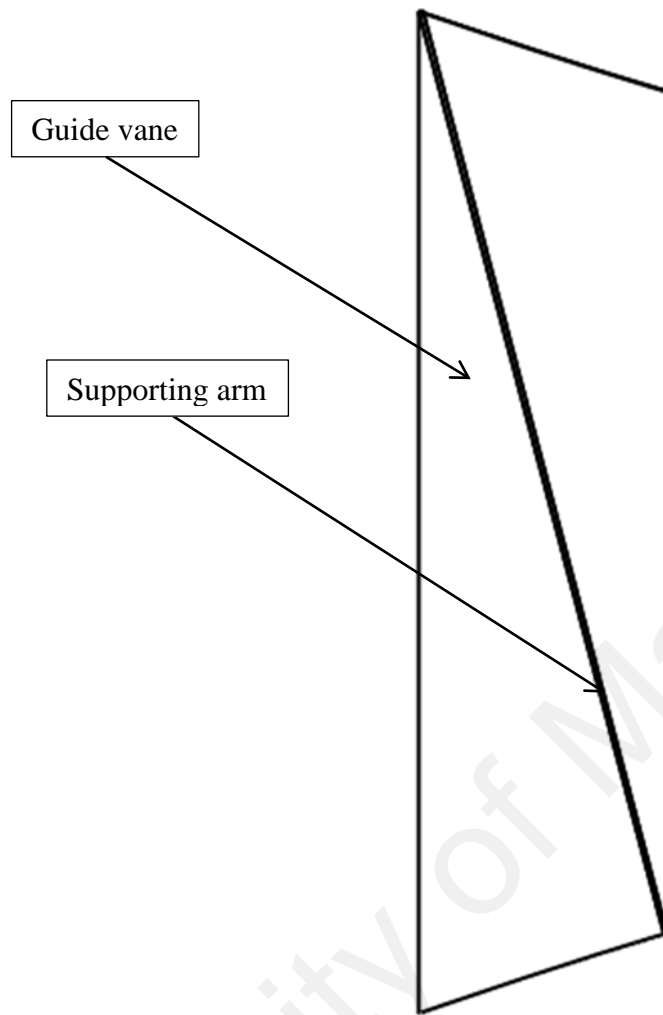


Figure 4.5: Side view of a vane and its support

The shown guide vane is designed to be bolted on the upper wall duct and down plate of the PAGV. Consequently, rectangular hollow bar arms support all the guide vanes of the PAGV in order to form the final design of the PAGV. The lower duct of the PAGV is welded on the base support (Figure 4.6), which can be without difficulty connected to the floor. Figure 4.6 shows the Base supports proposed for the PAGV.

In fact, lower duct, upper duct and guide vane have the capacity to be produced individually and assembled at the desired place, which makes the PAGV easy to be transferred and applied in different situations.

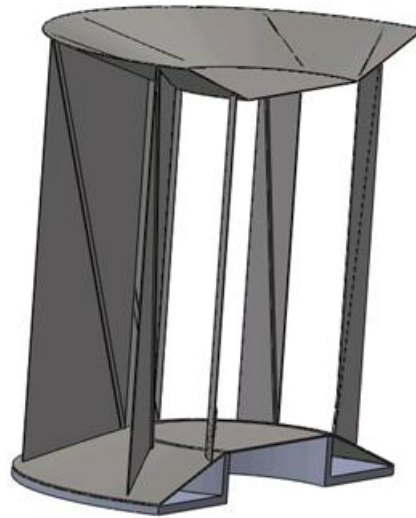


Figure 4.6: Sectional view of the PAGV with base support

4.5 Computational Scope

The area of analyzing problems by computer is often limited to more common commercial software such as ANSYS, Fluent, Abaqus, and Nastran and so on. In this paper, specifically in order to inspect the behavior of PAGV, Gambit, Fluent and ANSYS are adopted. In addition, SolidWorks is the main CAD software for designing the PAGV and importing it into the desired analyzer software. Indeed, the analysis is divided into two main sectors of fluid and solid inspections. Although, ANSYS software version 12 is able to do both solid and fluid analyzing, to have more precise answers, special software for each section is adopted.

The process of analyzing is categorized into three steps, which are:

- Using ANSYS to define boundary condition
- Using ANSYS Fluent to find out pressure profile
- Using ANSYS to define the structure behavior under wind pressure

4.5.1 Contours of Pressure

The prerequisite to obtain the results of structural analysis is to calculate the pressure profile. In order to define pressure profile the CFD simulation is performed. Generally, A CFD simulation consists of three main steps, which are preprocessing, solving and post processing. The first step is to build and analyze a flow model. It includes building the model by CAD software, preparing and applying a proper computational mesh and defining and allocating boundary conditions and material properties of the fluid. In the second stage, which is solving, CFD prepares flow calculations and produces the results. Post processing is the final step in CFD analysis, involving the organization and interpretation of the predicted flow data and the production of CFD images and animations.

4.5.2 Wind Domain

To create a wind domain, ANSYS Design Modeler and ANSYS Mechanical are applied to create a computational discretized meshed domain, which is ready to be simulated. To simulate the PAGV, two rectangular computation domains are defined. The outer rectangular is six times bigger in x and y direction and five times bigger in z direction while the inner rectangular is one and half time bigger than the PAGV. Indeed, the inner rectangular is a hypothetical domain, which is merely created due to the dimension of the wind domain that is too huge to be simulated by normal computers. It is difficult for computers to simulate such a huge domain so; the inner rectangular domain assists us to tackle this problem. In addition, the wind domain dimension is to be carefully defined to have computational free stream so that the far field free stream is not affected by the flow near the PAGV. The wind domain is situated so that the PAGV is placed at the center and the inlet flow is set far enough in front of the PAGV to allow the flow becoming fully developed when it reaches near the PAGV. The inlet is set approximately three times of the

subject diameter further from it. In a similar way downstream is set as the same before it reaches the outlet. In fact, to be able to analyze the turbulence occurring at the time when flow is leaving the PAGV, an adequate long downstream is required. Figure 4.7 and Figure 4.8 show the isometric view of the PAGV and wind domain.

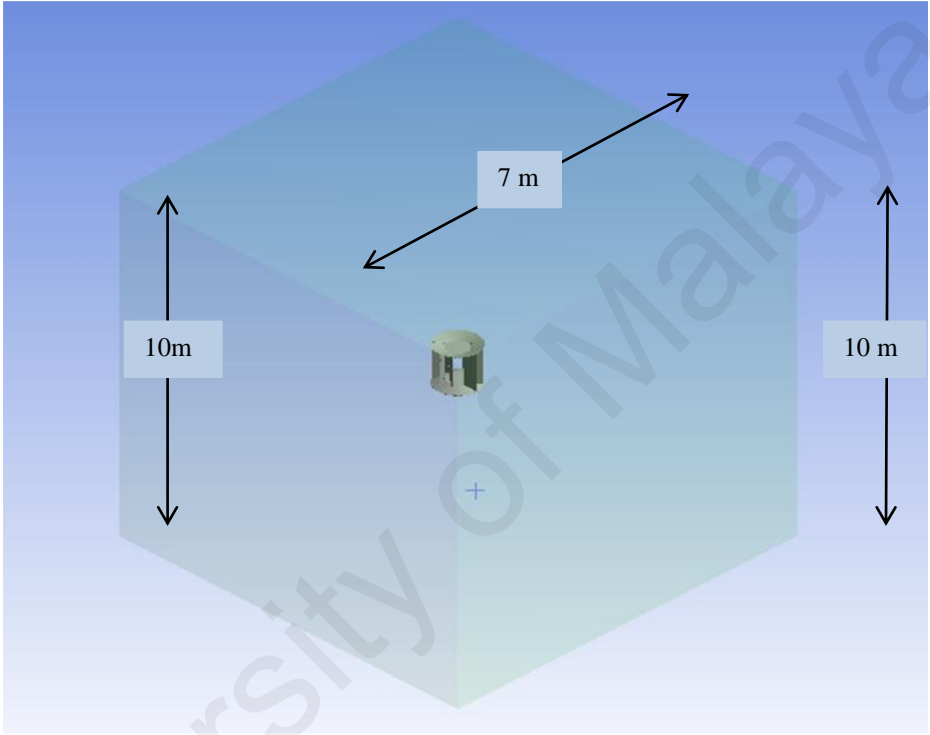


Figure 4.7: Wind domain created for simulation

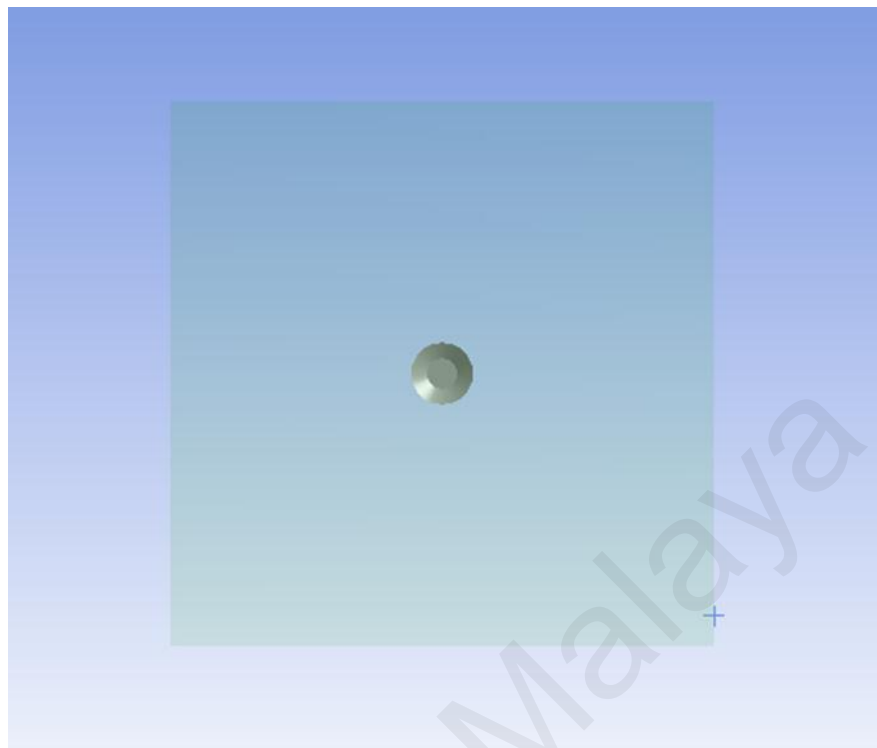


Figure 4.8: Top vie of wind domain

However, before calculating the pressure profile, carefully defining the boundary conditions of the computational domain is the main issue in order to obtain the most accurate results.

4.5.3 Boundary Conditions

Boundary conditions define the characteristics of thermal and fluid flow variables. Therefore, boundary conditions are the most important issue in the process of simulating flow problems. As a matter of fact, one of the advantages of ANSYS Fluent software is its comprehensive boundary conditions menu, which enables users to simulate most industrial problems.

4.5.3.1 Define Boundary Conditions

From the zones panel prepared by ANSYS Fluent software, we are able to make the initial setting for defining boundary conditions. In order to do so, all the faces of the wind

domain must be properly named. Among these boundary conditions some are interchangeably used and some only specifically. Since the airflow is incompressible, the inlet boundary condition is set to velocity inlet, while the outlet is defined as outflow.

In fact, out-flow boundary conditions are used when details of the flow properties namely the velocity and pressure are prior unknown to the solution of the flow problem. Although, out-flow boundary condition is only suitable for a fully developed flow, the exit flow distance is far more adequate from the PAGV to have the fully develop flow velocity profile. Four other sides of computational domain including the up, front, back and bottom of the outer rectangular domain and the PAGV model are set as wall boundary type. Wall boundary conditions are used to bind the fluid regions.

In this case, a smooth wall is modeled without any rough areas. Such a condition can be met by dying all surfaces with smooth paint. Finally, all faces of the inner rectangular are set to be interior. Figure 4.9 shows the velocity inlet, A, and outflow, B conditions. Hatched areas shown in the Figure 4.10 show the wall type boundary condition.

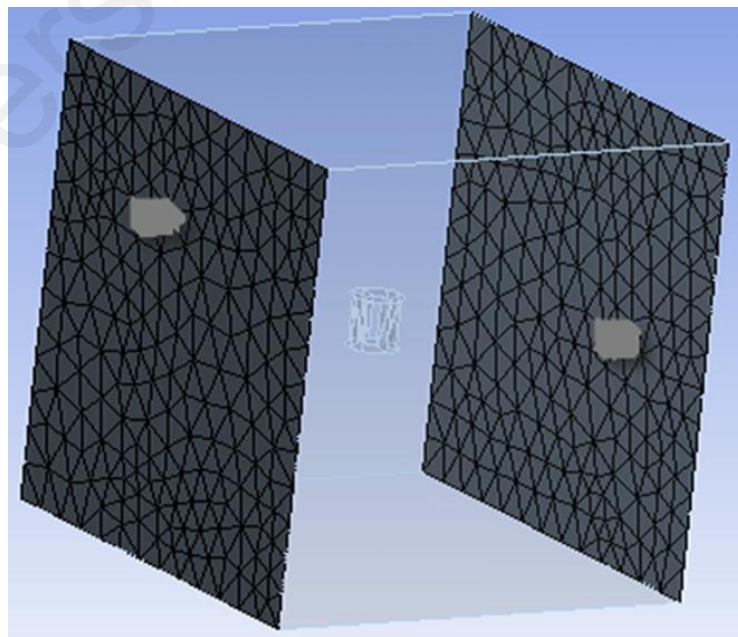


Figure 4.9: Boundary condition (velocity inlet and outflow)

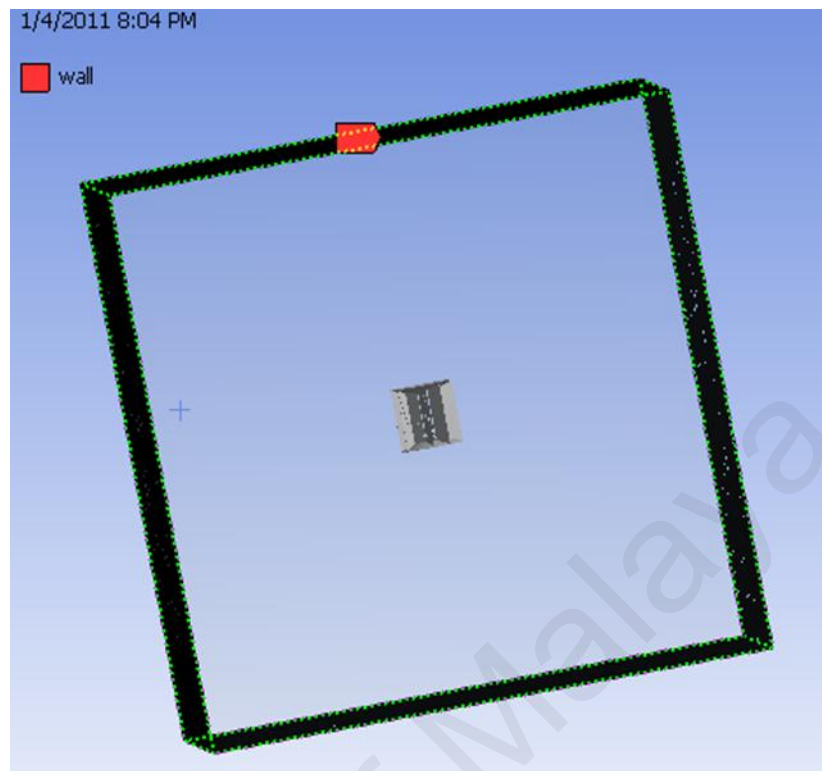


Figure 4.10: Boundary condition (walls)

4.5.4 Mesh Process

To mesh models is important because the accuracy of the solution is highly dependent upon the mesh quality. Therefore, the coarser, mesh selected definitely delivers less reliable results. In this paper, mesh is begun with the surfaces and it is completed with meshing volumes. First of all, the entire PAGV surface is meshed with the interval of six millimeters. After that, size function with default growth rate (1.2) and size limit (100) is applied to mesh the inner rectangular computational domain. That means the size of mesh elements is growing at a rate of 1.2 from the interval size of six on the PAGV surfaces until the maximum size of 100 on the surfaces of the wind domain during volume meshing. In a similar way, the outer rectangular volume is meshed. Obviously, the coarse mesh of the outer rectangular will not affect the calculations.

The Tetrahedral/Hybrid is selected as volume mesh element. This element specifies that the mesh composed of tetrahedral elements and may include hexahedral, pyramidal, and wedge elements where appropriate. When geometries are complex or the range of length scales of the flow is large, a triangular/ tetrahedral mesh can be created with far fewer cells than the equivalent mesh consisting of quadrilateral/hexahedral elements. This is because a triangular/tetrahedral mesh allows clustering of cells in selected regions of the flow domain. Structured quadrilateral/hexahedral meshes will generally force cells to be placed in regions where they are not needed. Therefore, setup time for complex geometries is the major motivation for using unstructured grids applying triangular or tetrahedral cells.

As a matter of fact, to make sure about the quality of mesh skewness should be checked out. Skewness is the difference between an element cell shape and an equilateral cell of the same volume. Optimal quadrilateral meshes are defined as having vertex angles close to 90 degrees, while triangular meshes preferably have angles of close to 60 degrees and have all angles less than 90 degrees. High skewness of the meshing cell is undesirable, as it has a significant impact on the numerical solution accuracy and convergence. For an accurate analysis, the skewness of an individual mesh element has to be less than 0.97. To avoid this problem, the PAGV is simplified to a relatively smoother geometry with less small feature but its streamline body shape is maintained. Figure 4.11 shows the outer rectangular mesh. However, the mesh seems coarse the quality of mesh consistently increases as we get closer to the PAGV as can be seen in the cut view shown in the Figure 4.12.

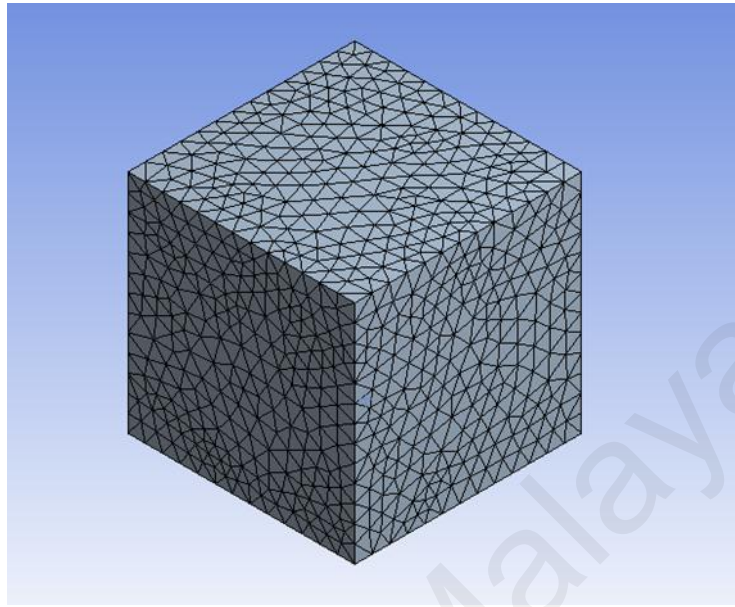


Figure 4.11: Mesh created for the wind domain

Figure 4.12 shows three dimensional cut view of the quality of mesh. As is illustrated, the mesh quality remarkably increases around the PAGV, which is significant to achieve a more reliable simulation.

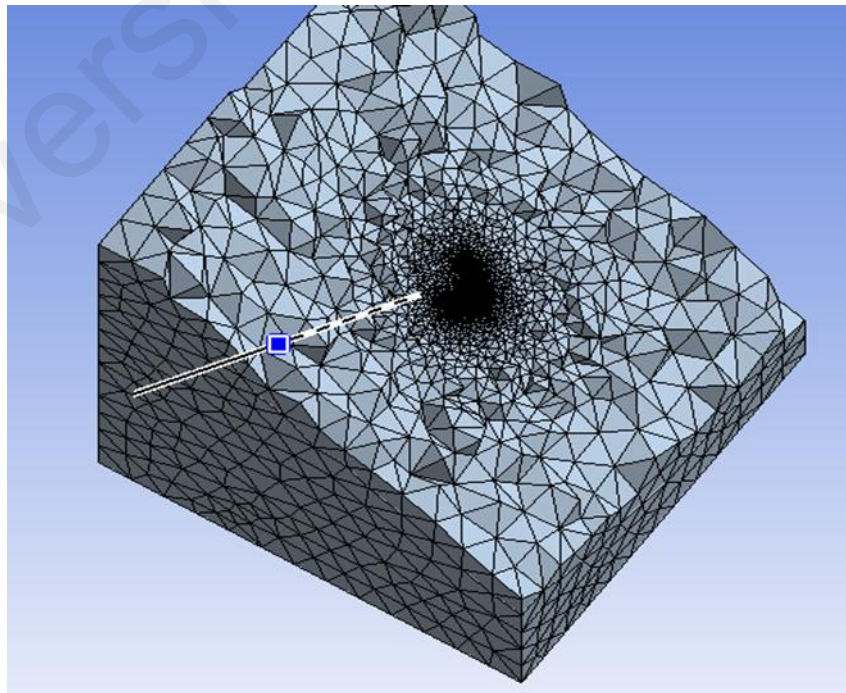


Figure 4.12: Three dimensional mesh cut view

ANSYS Fluent provides an even better comprehension of the diversity of mesh quality for the wind domain. Figure 4.13 shows quality of the mesh throughout the wind domain. It shows that most of the 854356 elements have the skewness less than 0.50, which is indicative of the acceptable mesh quality. The skewness is defined as the ratio of the difference between optimal mesh size and the cell size to the optimal mesh size.

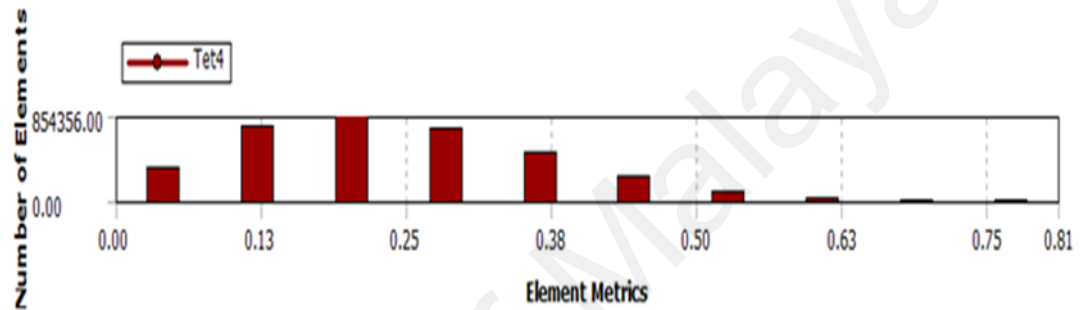


Figure 4.13: Mesh diversity through the PAGV

4.5.5 Turbulence Model Parameters

Among the turbulence models of Fluent software, the Realizable $k-\varepsilon$ model is chosen due its robustness, economy, and reasonable accuracy making it the most popular model in industrial simulation. The $k-\varepsilon$ model is often used for stationary problems and when the surface curvature is negligible. Janajreh et al. (2010) used $k-\varepsilon$ model in order to investigate the flow field for a downstream wind turbine. They found good agreement between numerical and experimental results. Besides, the $k-\varepsilon$ model as a widely used model to simulate wind turbines and wind farms has been used by researchers in order to simulate wind turbines and wind farms (Crespo, 1999). The main purpose of performing CFD analysis in this paper is to obtain the pressure profile, which is the first step of structural analysis. Therefore, for the current investigation the Realizable $k-\varepsilon$ model is adopted to

simulate the PAGV. Figure 4.15 shows the contours of total pressure obtained by realizable $k-\varepsilon$ models.

In ANSYS Fluent the scalar magnitudes related to turbulent flow must be defined at inlet, outlet and far field boundaries. However, in fully developed turbulence flow, if it is not necessary to exactly define these parameters at the mentioned boundaries, it is possible to determine the parameters by profiles prepared from experimental tests or experimental formulas. In addition, in ANSYS Fluent it is possible to address these profiles to the chosen turbulence model. Nevertheless, in some problems it is more suitable to give constant magnitudes to turbulence parameters. For instance, in problems such as flow in ducts, far fields and even a fully developed flow in the canal turbulence, parameters can be assumed constant. In fact, turbulence parameter that is taken into account for PAGV can be classified as:

- Hydraulic Diameter
- Turbulence Length Scale

However, for a rectangular duct, which is completely filled with fluid the following experimental formula, is applied to calculate the hydraulic diameter (D_h):

$$D_h = \frac{4LW}{2(L+W)} = \frac{2LW}{L+W} \quad (17)$$

The turbulence length scale l is a physical quantity related to the size of the large eddies that contain the energy in turbulent flows. In fully developed duct flows, l is restricted by the size of the duct because the turbulent eddies cannot be larger than the duct. An approximate relationship between l and the physical size of the duct is:

$$l = 0.07L \quad (18)$$

After entering the initial parameters such as wind velocity, hydraulic diameter and turbulence, the convergence was defined. The accuracy is further improved by applying the second upwind scheme discretization method for the momentum, turbulence kinetic energy and turbulence dissipation rate. The computation was initialized from the velocity inlet and the solution is converged after it iterates until 437 times. Figure 4.14 shows the convergence history of Realizable $k-\epsilon$ model.

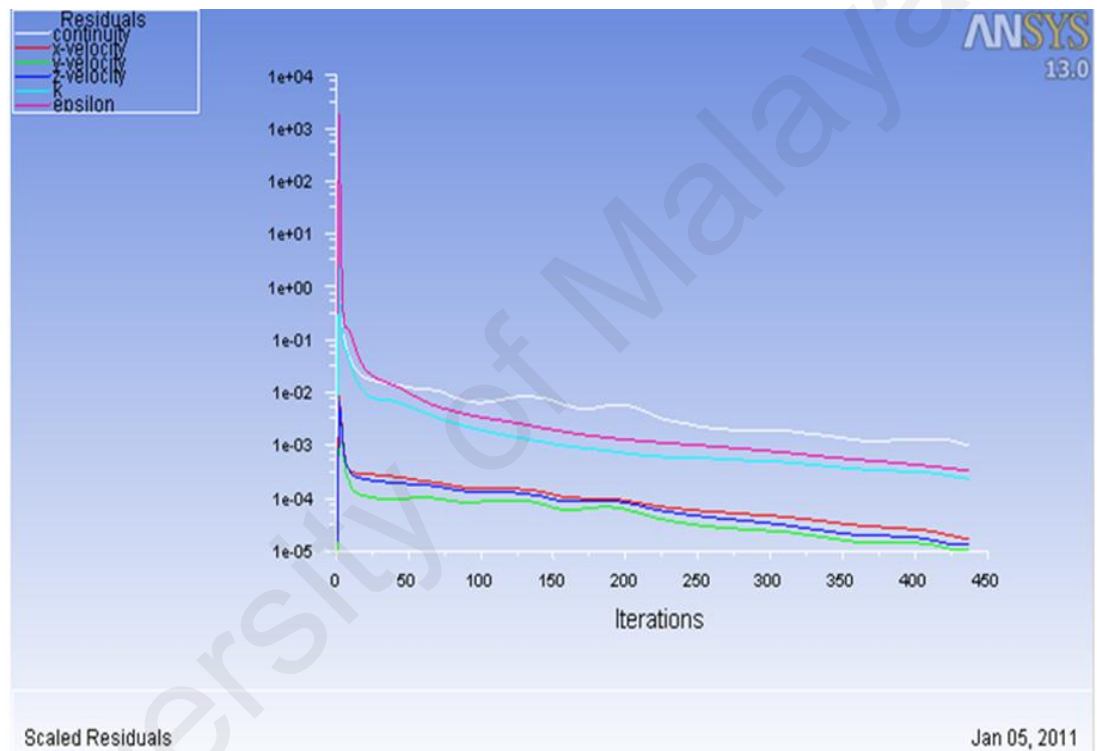


Figure 4.14: Iteration process

Figure 4.16 shows the velocity vectors obtained by the realizable $k-\epsilon$ model respectively.

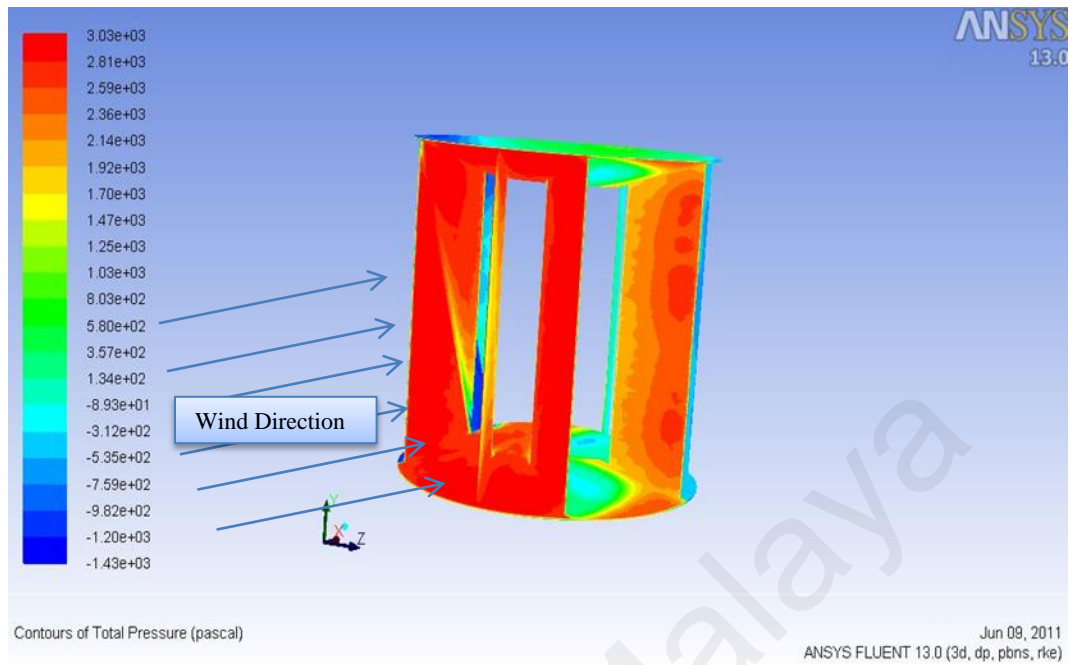


Figure 4.15: Contours of total pressure on the PAGV obtained by realizable $k-\varepsilon$ model

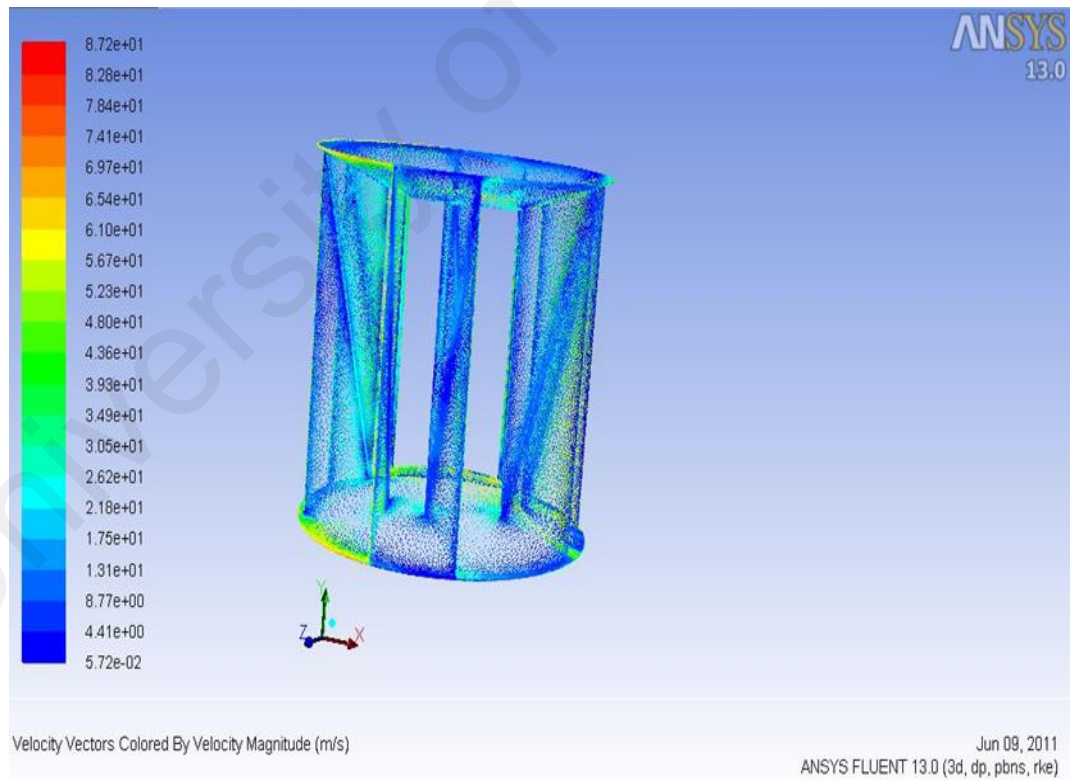


Figure 4.16: Velocity vectors colored by velocity magnitude (m/s) obtained by realizable $k-\varepsilon$ model

4.6 Static Structural Analysis

To accomplish the structural analysis selecting the proper software to perform the analysis is a significant factor in order to reach reliable results. Among the finite elements based software, ANSYS is adopted due to its compatibility with the previous calculation done by Fluent. Therefore, ANSYS version 12 integrated with Workbench will be the solver for the structural analysis.

In general, there are three ways of performing analysis by ANSYS version 12 and above.

- To use Workbench
- To use Mechanical APDL (Black ANSYS)
- To apply a combination of Workbench and Black ANSYS

Although the first method, which uses Workbench, delivers acceptable results; it is not commonly applied by users because of its novelty. Indeed, Workbench is more comfortable and effective in comparison with Black ANSYS since it offers more options and also the ability to manage the project during the process of analyzing the problems. However, using Mechanical APDL is also reliable and effective. In particular, its command line enables users to input parameters, which make the Black ANSYS results transformable and more reliable. But its disadvantage is to solve assemblies' problems which required a lot of time to define connections manually, while Workbench is able to perform this in much shorter time.

The third method which is recommended by ANSYS Inc. is the most effective and most reliable to engineering problems. However, in the present paper due to the computer capabilities, the first method is preferred to others.

However, to perform static structural analysis of the PAGV is mainly subject to mapping the obtained pressure profile to the PAGV. Since the pressure profile was obtained by ANSYS Fluent, the initial setting of the static structural is directly imported from the ANSYS Fluent.

In fact, fluid structural analysis (FSI) has been added to ANSYS package¹². So, the process of analyzing the PAGV is categorized to following steps:

- a) To link ANSYS Fluent to ANSYS structural
- b) To define the material properties
- c) To define element properties and create proper mesh
- d) To define supports' loads
- e) To set the refine parameters
- f) To solve the model and view the results

However, before starting the structural analysis it is necessary to check the unit system of the Fluent and structural ANSYS in order to avoid any unmatched units. The unit system is set to be SI whereas the length unit is the millimeter.

4.6.1 Connecting Analyzing Systems

ANSYS Workbench provides a set of analysis systems such as static, thermal and so on. Besides, all of the analysis systems containing some cells like material data set up, solution and so on. Each cell of the select analysis system has the capability to be connected to another analysis system cell. In addition, the properties of connections also are provided in a different window. Figure 4.17 shows analysis configuration in ANSYS-Workbench 13.

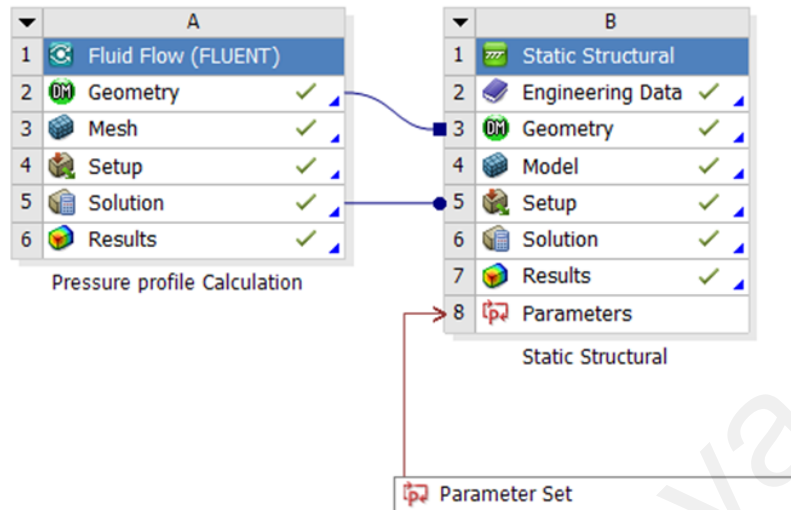


Figure 4.17: Connecting ANSYS Fluent to ANSYS Static Structural

4.6.2 Engineering Data

The first step of the analysis is to define the proper material. ANSYS-Workbench provides a wide set of materials, which are available at engineering data cell. Table 4.2 shows the material properties of the select material to initiate solving the problem.

Table 4.1: Mechanical properties of the select material (TM 460)

1	Property	Value	Unit
2	Density	7850	kg m ⁻³
3	Isotropic Secant Coefficient of Thermal Expansion		
4	Coefficient of Thermal Expansion	1.2E-05	C ⁻¹
5	Reference Temperature	27	C
6	Isotropic Elasticity		
7	Derive from	Young's Modulus and Poisson's Ratio	
8	Young's Modulus	2.05E+11	Pa
9	Poisson's Ratio	0.29	
10	Bulk Modulus	1.627E+11	Pa
11	Shear Modulus	7.9457E+10	Pa
12	Alternating Stress Mean Stress	Tabular	
16	Strain-Life Parameters		
24	Tensile Yield Strength	6.25E+08	Pa
25	Compressive Yield Strength	5.3E+08	Pa
26	Tensile Ultimate Strength	8E+08	Pa
27	Compressive Ultimate Strength	0	Pa

4.6.3 Modeling

Workbench provides a set of mesh controllers to adjust the mesh factors such as element shape, element size and so on. The default mesh controls used by the program may produce a mesh that is adequate for some models. In that case, it is not necessary to specify any mesh controls. However, in the PAGV case mesh controls are set before meshing the solid model. This step is one of the most important parts of the entire analysis, which will profoundly affect the accuracy, and economy of the analysis. In fact, volume elements are often either hexahedral (brick) or tetrahedral shaped, but a mixture of the two shapes in the same model is not recommended.

In order to set the appropriate mesh for the PAGV in ANSYS-Workbench the first necessary step to define is to determine the physical preference in Mechanical. Figure 4.18 shows the mesh properties menu in ANSYS-Workbench 13.

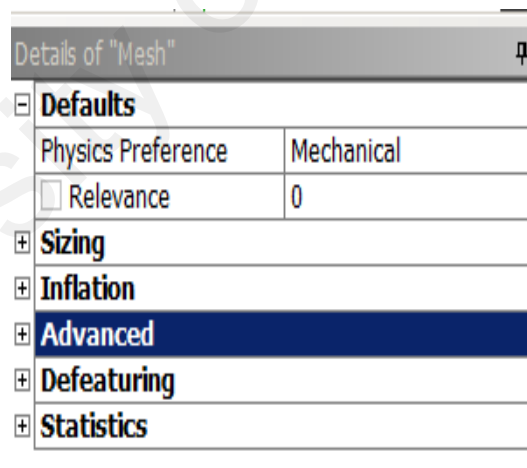


Figure 4.18: Mesh properties window (ANSYS-Workbench 13)

In addition, the mesh method must be carefully defined. Workbench automatic patch conforming under Tetrahedrons was selected for this project. To increase the likelihood of a successful mesh, the material behavior is set to soft, which means proximity, curvature, and local re-meshing during the meshing process will affect the size control. Besides, it also

means that the size or number of divisions is not fixed on the edge and can be changed by the meshing algorithm. In addition, the Advance Size function was selected due to its greater control over mesh process. It is used to control the following properties:

- Angles between Normals for adjacent mesh elements (curvature-type size functions)
- Number of mesh elements employed in the gaps between two geometric entities (proximity-type size function)
- Gradation between minimum and maximum sizes based on a specified growth rate

However, proximity and curvature size function are applied for this project because of the characteristics of the PAGV shape. The most significant part of the Advance Size function is setting a value for minimum size. Choosing extra small minimum size may lead to an unnecessarily fine mesh and longer meshing time. On the other hand, setting a value that is too large may mean that important features are not captured by the mesh. Therefore, the minimum size of the element for the PAGV was set at 4 millimeters and the maximum size of the face also was set at 80 millimeters. In addition, the maximum element size was set at 160 millimeters and the growth rate at 1.5. The proximity size function allows us to specify the minimum number of element layers created in regions that constitute gaps in the model. A gap includes internal volumetric region between two faces or the area between two opposing boundary edges of a face.

The curvature size function that examines curvature on edges and faces in order to compute element sizes on these entities so that the size will not violate the maximum size or the curvature normal angle. The process of meshing produced 1131306 elements. Figure 4.19 shows details of the PAGV provided by ANSYS-Workbench 13. An isometric view of the meshed PAGV was shown in the Figure 4.21.

Details of "Mesh"	
Defaults	
Physics Preference	Mechanical
<input type="checkbox"/> Relevance	0
Sizing	
Use Advanced Size Function	On: Proximity and Curvat...
Relevance Center	Fine
Initial Size Seed	Active Assembly
Smoothing	High
Transition	Slow
Span Angle Center	Coarse
<input type="checkbox"/> Curvature Normal Angle	Default (70.3950 °)
<input type="checkbox"/> Proximity Accuracy	0.5
<input type="checkbox"/> Num Cells Across Gap	Default (3)
<input type="checkbox"/> Min Size	4.0 mm
<input type="checkbox"/> Max Face Size	80.0 mm
<input type="checkbox"/> Max Size	160.0 mm
<input type="checkbox"/> Growth Rate	1.50
Minimum Edge Length	9.1073e-002 mm
Inflation	
Advanced	
Defeaturing	
Statistics	
<input type="checkbox"/> Nodes	2254205
<input type="checkbox"/> Elements	1131306
Mesh Metric	Skewness
<input type="checkbox"/> Min	9.09357377588793E-04
<input type="checkbox"/> Max	0.976757460962366
<input type="checkbox"/> Average	0.330796034640483
<input type="checkbox"/> Standard Deviation	0.139635141862837

Figure 4.19: Mesh properties

The quality of mesh can be seen in the above picture. Figure 4.20 delivers more details about the mesh quality.

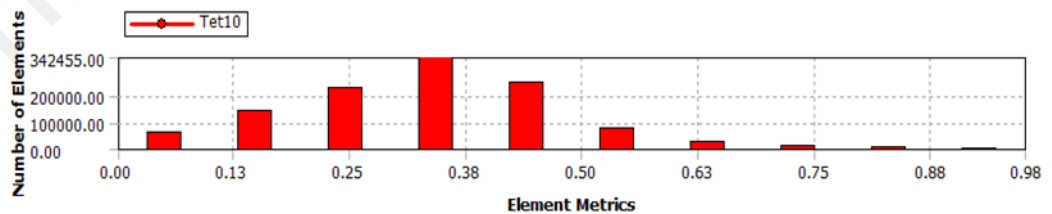


Figure 4.20: The PAGV mesh skewness

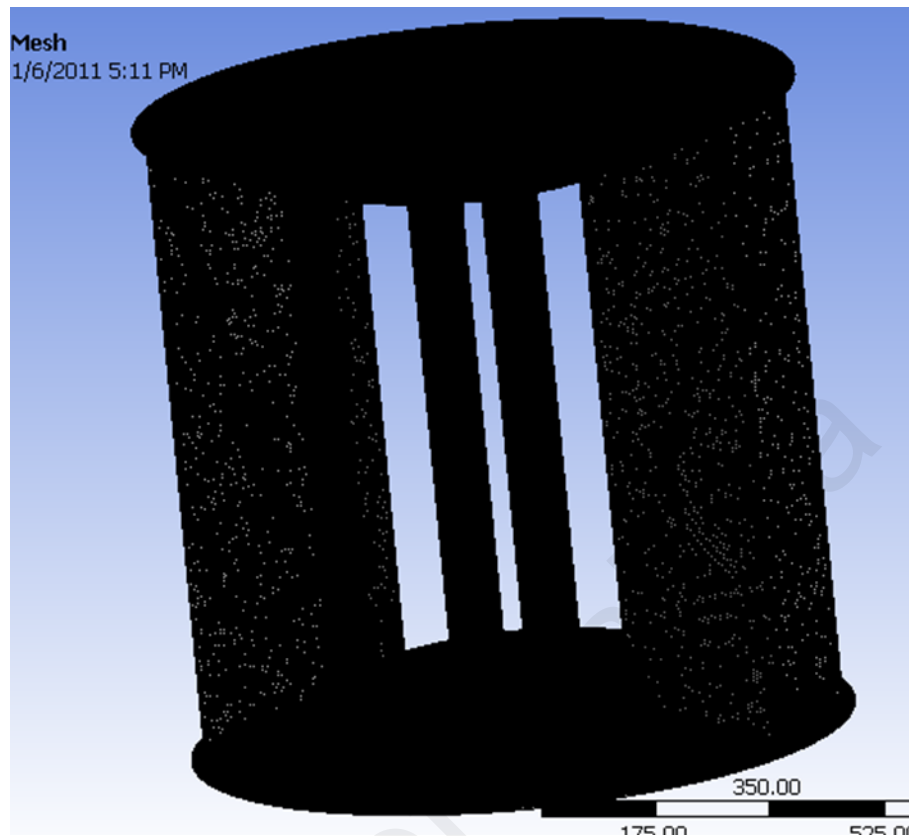


Figure 4.21: The PAGV mesh

4.6.4 Analysis Setting

A static structural analysis determines the displacements, stresses, strains, and forces in structures or components caused by loads that do not induce significant inertia and damping effects. Steady loading and response conditions are assumed; that is, the loads and the structure's response are assumed to vary slowly with respect to time. A static structural load can be performed using the ANSYS solver.

For simple linear static analyzes typically there is no need to change default settings. For more complex analyzes such as the PAGV, the basic controls are a Large Deflection and step control. Typically, for slender structures that are assumed to have transverse displacements of more than 10% of the thickness the Large Deflection option must be chosen.

4.6.5 Loads and Supports

In order to solve the problem, the next step is to define the structural loads and supports. The effect of the PAGV weight is not taken in to account, so that the only load for the current problem is the wind pressure, which has already been calculated. In ANSYS-Workbench, not only we are able to apply constant pressure loads or force vectors per unit area, but also to utilize hydrostatic pressure loads and line pressure loads. Moreover, there are various options to applying fluid pressures such as mapping from a steady-state transient ANSYS Fluent solution or to import a predefined spatially-varying pressure field from an external text file. Nevertheless, in this paper the pressure profile was directly mapped from ANSYS Fluent to ANSYS-Structural. However, the computer spent more than 70 hours to accomplish the mapping pressure profile. Figure 4.22 shows the wind pressure on the PAGV surface.

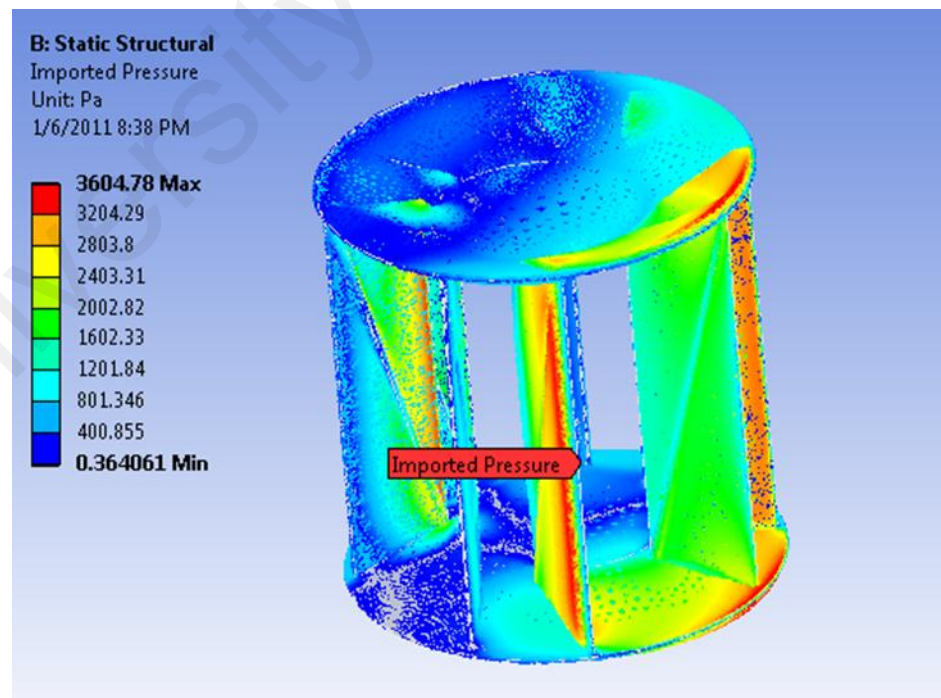


Figure 4.22: The pressure applied on the PAGV, where the lower duct is fixed

4.6.6 Solving the problem

This step initiates the solution process. The overall procedure for obtaining a solution in the Mechanical application is as follows:

- Specify the type
- Initiate the solution

In addition, the relative accuracy of a solution can be controlled in two ways. It is possible to use the meshing tools to refine the mesh before solving, or apply convergence tools as part of the solution process to refine solution results on a particular area of the model. Regardless the mesh tool was chosen to increase the accuracy result because the convergence is not supported for result objects that belong to linked analyses, or an imported load object exists in the environment.

At the same time, solver type can be defined using Program Controlled, Direct, or Iterative solvers. A direct solver works better within flexible models. An iterative solver works better for bulky models. For the PAGV the solver type is controlled by the program to select the optimal solver.

To initiate solving structural problem the following objects were considered to be solved:

- Set up the fixed supports
- Stress (equivalent)
- Strain (equivalent)
- Deformation

Stress solutions are to predict safety factors, stresses, strains, and displacements for a particular structural loading environment. Equivalent (Von Mises) stress and strain which are based on the maximum equivalent stress failure theory referred to as the Von Mises-Hencky theory was selected to calculate the stress and strain in order to predict yielding in a

ductile material. Equivalent stress is often used in design work because it allows any arbitrary three-dimensional stress state to be represented as a single positive stress value.

The edges of the lower duct of the PAGV were supposed to be welded on the base support shown in the Figure 4.6. The fixed supports for the mentioned condition are illustrated at Figure 4.23.

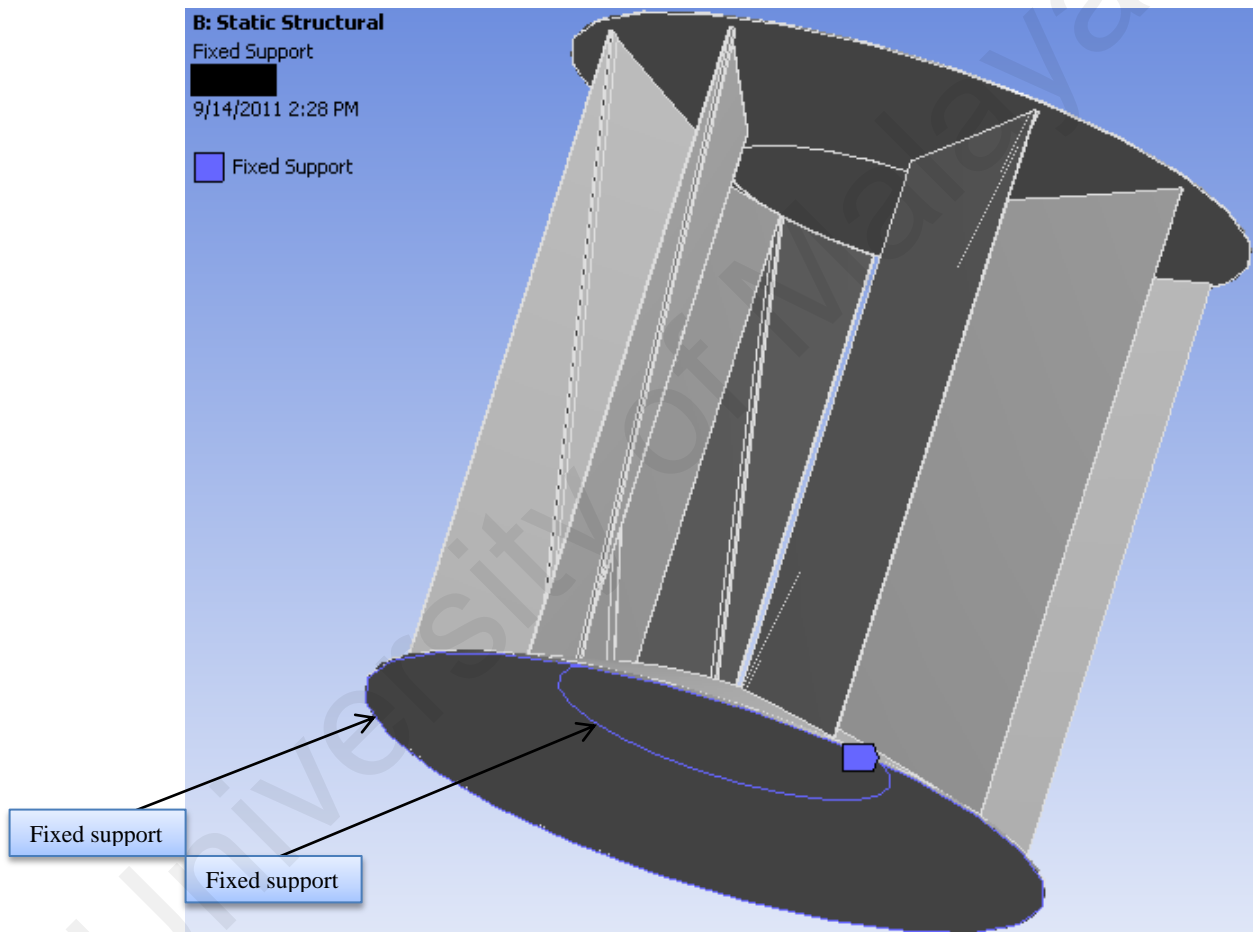


Figure 4.23: Fixed supports of the PAGV

CHAPTER 5

RESULTS AND DISCUSSION

In this chapter, results are presented for the PAGV made of High-strength low-alloy steel (TM 460) exposed to wind velocity. The British Standards of BS 5950 and BS 6399: part 2, was used In order to calculate the effective wind speed. For calculating the effective wind speed the below formula was introduced by the BS5950.

$$V_e = V_s \cdot S_b$$

Where V_s is the site wind speed and can be obtained by:

$$V_s = V_b \cdot S_a \cdot S_d \cdot S_s \cdot S_p$$

Where, S_a , S_b , S_d , S_s , S_p are respectfully, altitude factor, structure and terrain factor, directional factor, seasonal factor and probability factor.

The terrain and building factor S_b is determined directly from Table 4 of BS 6399: Part 2, depending on the effective height of the building and the closest distance to the sea. The altitude factor S_a depends on whether topography is considered to be significant or not, as indicated in Figure 7 of BS 6399: Part 2. When topography is not considered significant, by considering Δs , the site altitude (in meters above mean sea level), S_a should be calculated. The directional factor S_d is used to adjust the basic wind speed to produce wind speeds with the same risk of being exceeded in any wind direction which is generally considered to be 1. The seasonal factor S_s is used to reduce the basic wind speed for structures which are exposed to the wind for specific subannual periods. The seasonal factor is considered to be 1, for structures exposed to the wind for a continuous period of more than 6 months. The probability factor S_p is used to change the risk of the basic wind

speed being exceeded from the standard value annually. For normal design applications, S_p may take a value of 1. Therefore the effective wind speed can be obtained as below:

$$V_e = 27 \times 2.17 \times 1 \sim 60 \text{ m/s}$$

Where, $S_b = 2.07$ (table 4, BS-6399 part: 2), $V_b = 29 \text{ m/s}$ (table 3.1, MS 1553).

Therefore, based on the wind speed of 60 m/s results produced by ANSYS solver were used to evaluate the effects of the wind pressure on the PAGV. The simulation results generally are provided in three main parts:

- Stress
- Deformation
- Strain

Furthermore, the result can be benchmarked with different material by changing the parameter, which has been set during the analysis setting.

5.1 Stress Results

Solver results for the stress illustrate that the maximum stress induced by wind pressure happens at the place where the supporting arms are connected to the PAGV bottom plate. In fact, the maximum stress is the most significant factor to consider where selecting the proper material. The following picture illustrates the stress over the PAGV. However, the lower wall duct exposes minimum stress while the upper wall duct tolerates unremarkable stress in particular at the places where the guide vanes are connected to the plate. The simulation results show that the minimum safety factor of the proposed PAGV design is equal to 1.7, which shows the material selected can be used under the defined conditions. Figure 5.1 shows the equivalent Von Mises stress provided by ANSYS. The minimum safety factor for the most critical parts equals to 1.73 for the proposed material (TM460) as it is shown below:

$$\text{Minimum safety factor} = \frac{\sigma_{max}}{\sigma_y} = \frac{530}{306.06} = 1.73$$

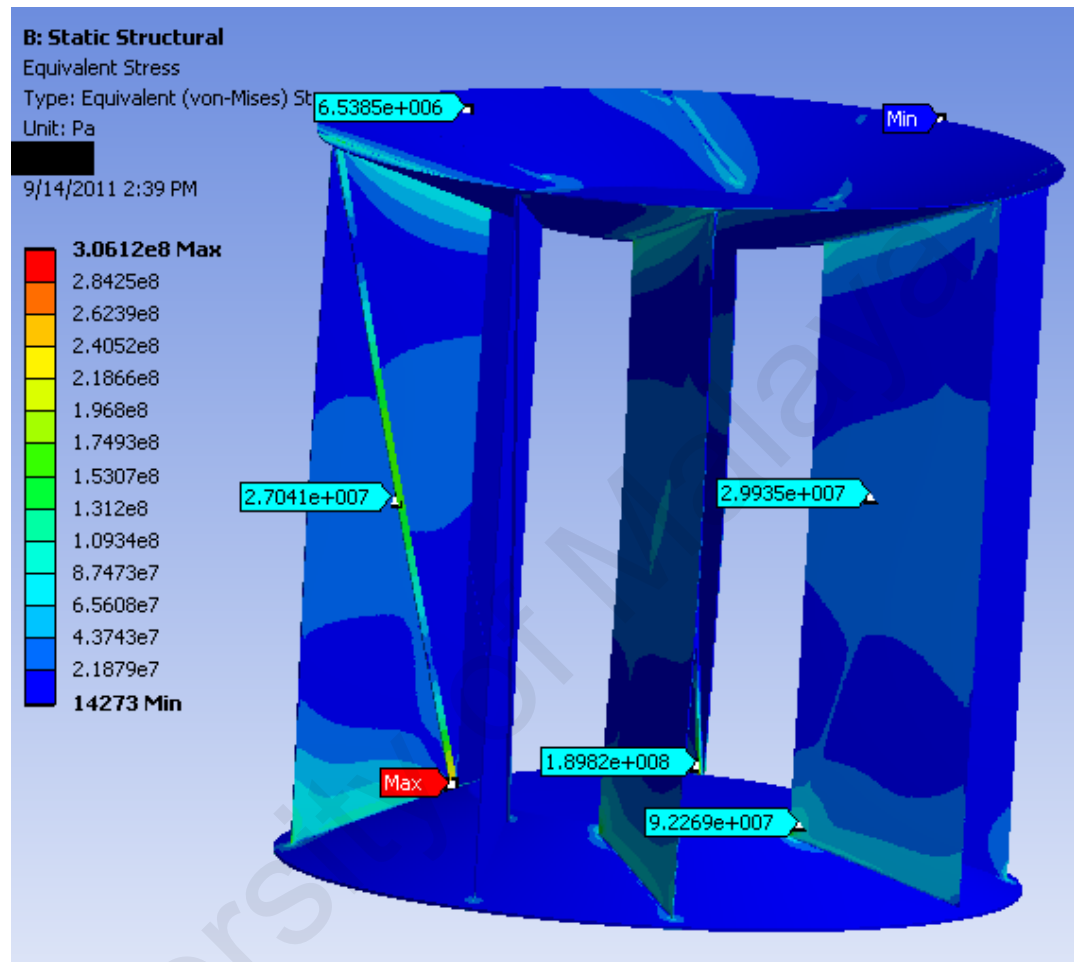


Figure 5.1: The equivalent Von-Mises stress distribution

5.2 Deformation results

Indeed, for slender designs the deformation is considered to be the most important factor. Nevertheless, the guide vanes of the PAGV with 2.5 mm thickness under the high pressure are predicted to become deformed. For the present PAGV design, results shows the maximum traverse deformation at the middle of the vane which is exposed to the direct fluid flow. Although a large deformation is expected because of the low thickness of the vanes, it also predicted to be an elastic deformation.

Figure 5.2 delineates the deformations of the PAGV caused by wind pressure. The maximum deformation equals to 9.46 mm occurring at the middle of the guide vans was observed.

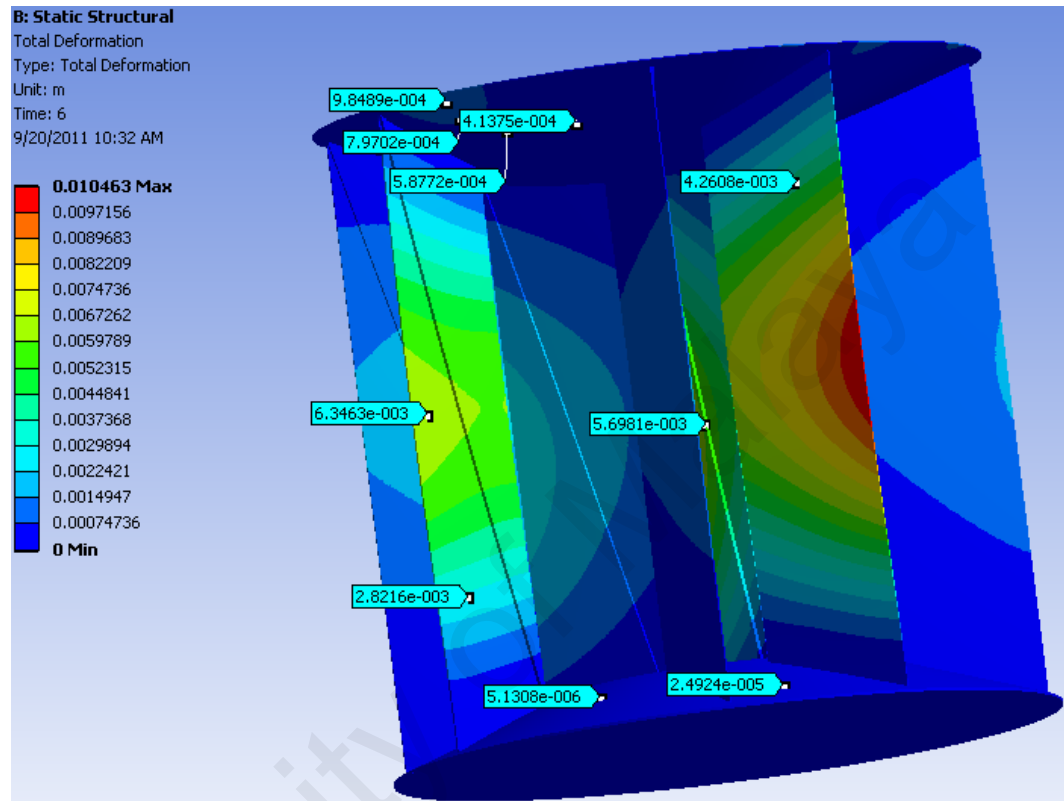


Figure 5.2: The PAGV deformation

5.3 Strain

The ratio of the dimensional change to original dimension is called strain. Most engineering materials undergo very small strain so the strain $\epsilon \ll 1$. Just as with stresses, strains are considered axial, or normal, if they occur in line with the applied load. These are termed tensile or compressive strains. If the deformation occurs parallel to the plane or area of applied stress, it is termed shear strain. In structural design ANSYS software uses the equivalent Von Mises stress to predict the failure. The stress strain relations can be used to convert the Von Mises criterion in terms of stresses into a criterion expressed in terms of

strains. However, the Mises criterion is form invariant between stresses and strains (Christensen, 2011).

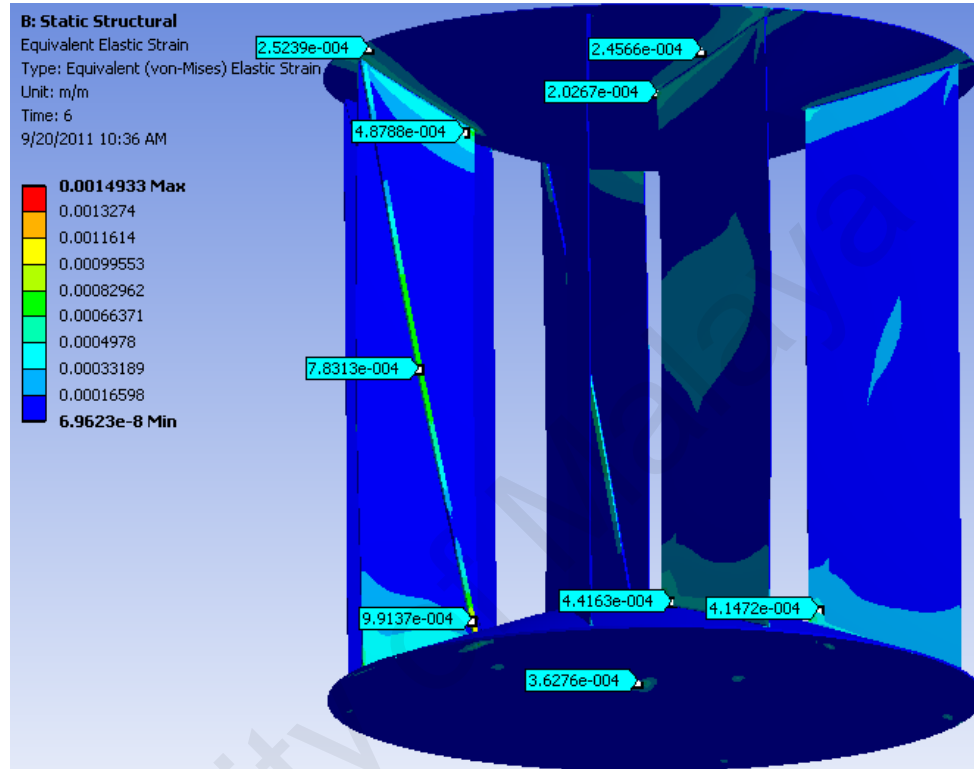


Figure 5.3: The elastic strain distribution of the PAGV

5.4 Discussion

At this point, the obtained solution from ANSYS is discussed and necessary suggestion is presented. Even though, the accuracy of the results could only be proven by an experimental work, in numerical methods the results are significantly depended on the mesh quality or the convergence accuracy. In order to analyze the PAGV the mesh dependency method was done. At first the default mesh produced by ANSYS software was accepted to perform the simulation. The mesh was refined and the process of simulation repeated until the consistent results were obtained.

In addition, the criteria used to select materials, which are exposed to high flow velocities are:

- Corrosion induced by high velocities, in particular erosion corrosion.
- Abrasion as metal loss caused by solid particles entrained by the fluid.

The obtained results prove that, the maximum Von Mises stress occurred at the points where the supporting arms are connected to the lower duct. The results obtained showed that the stress is far lower than yield stress of the select material in most of the structure. Therefore, it would be possible to use a different material with lower yield stress. If weaker materials are chosen, considerations need to be made in order to strengthen the connectors.

On the other hand, the results show a large deformation near the middle of the vanes. In order to overcome this deformation problem, the uniform strength plate is suggested in which the thickness of the vanes varies uniformly from the bottom and up to the middle (Brandt, 1986). The uniform strength plate can offer good mechanical properties particularly for the large deflection problems. The maximum thickness of 3.5 millimeter at the middle and minimum of 2 millimeter at the bottom and up is suggested for the current PAGV. Figure 5.4 illustrates a sectional view of the uniform strength plate recommended to be used as the vane.



Figure 5.4: Uniform strength vane

Another method to overcome the large deflection is to strengthen the vanes by using a particular support shown in the Figure 5.4.

As it is shown, the supports can remove the deflection problem but slightly increases the total weight of the PAGV. The supporting ring is made of separate parts that are bolted. This support can be added to the system at the last step of the setup of the PAGV. It is consisting of four parts illustrated in Figure 5.5 to 5.7.

To optimize the installation and also to reduce the movable parts it is recommended to manufacture the PAGV in two separate batches. The batches required to be separately assembled and installed on the site. The following pictures show the details of proposed design to overcome the deformation problem. Figure 5.8 shows the PAGV supported by the designed ring.

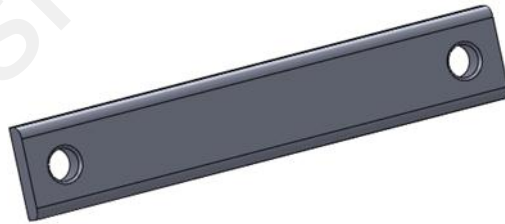


Figure 5.5: The deflection support component



Figure 5.6: Sectional view of the deflection support ring



Figure 5.7: The deflection support ring and attached to the connector disk

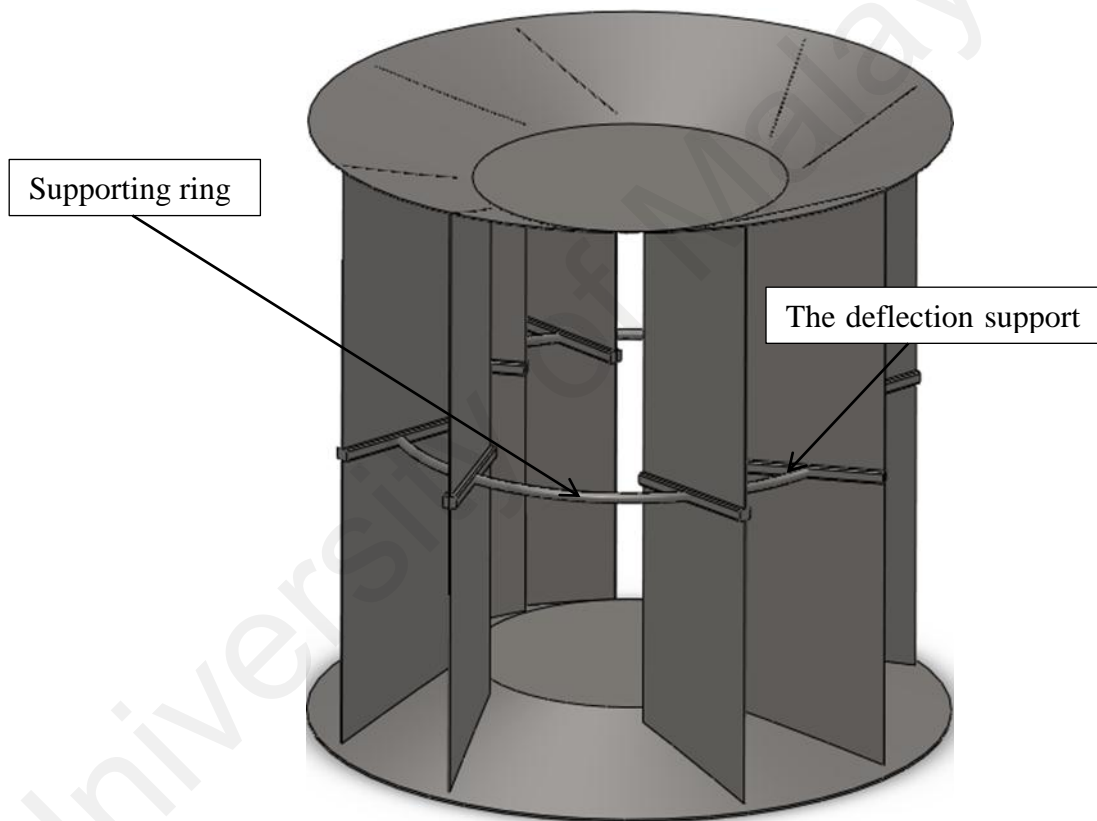


Figure 5.8: The PAGV and the proposed supports configuration

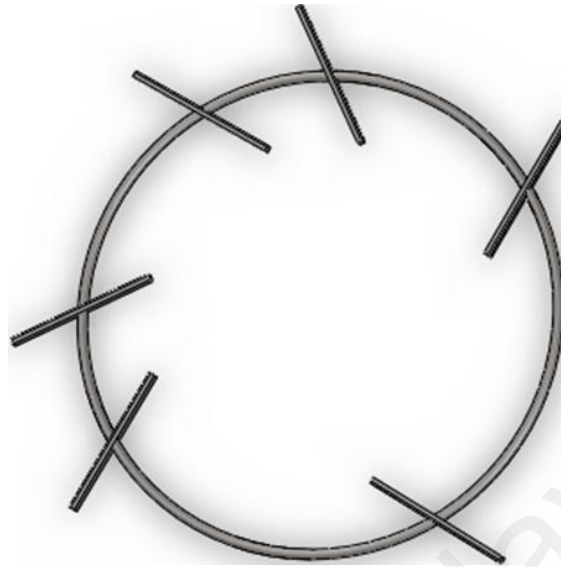


Figure 5.9: The designed support ring

In addition, based on the stress distribution obtained from the simulation it is possible to define various materials for different parts of the PAGV which maintain the minimum safety factor of 1.7 for the all structure. Table 5.1 classifies the High-strength low-alloy steel proposed for different parts of the PAGV and their applications based on the maximum stress of each part. The comprehensive properties of the proposed materials were studied by De Klerk and De Villier (1984).

Table 5.1: The PAGV material properties

Material	Component	σ_y (MPa)	σ_u (MPa)	E (MPa) $\times 10^3$	ν	σ_{max} \leq MPa	Elongation %
TM 420	Upper wall duct	490	700	203	0.3	250	20
TM 460	Guide vanes	530	700	203	0.3	306	20
TM 460	Supporting arms	530	625	203	0.29	306	20
TM 460	Lower wall duct	530	625	203	0.29	306	20

CHAPTER 6

CONCLUSIONS AND RECOMMENDATIONS

6.1 Conclusions

This project was performed to investigate the static structural behavior of the power augmented guide vane (PAGV) with 1020 mm, diameter and 2000 mm, height under pressure load of 3605 Pa, in real environmental conditions. The simulation was performed for the wind speed of 60 m/s which is calculated based on the British Standards of 5950 and 6399: part 2. The ANSYS software released 13 was used to simulate the pressure profile and structural loads.

The findings showed that the maximum stress equals to 306.1 MPa occurred at the places where the support arms are connected to the lower wall duct. The obtained safety factor shows that the material selected for the proposed PAGV can withstand the defined static loads. The supporting system suggested to overcome the large deflection appearing on the middle of the vanes will practically reduce the deflection to zero. It does not increase the total weight of PAGV considerably. The effects of additional supporting structure on the PAGV can be simulated in the future analysis.

6.2 Recommendations

Solutions obtained by the numerical methods are only delivering a prediction of the model behavior. In order to obtain the most reliable results it is strongly recommended to perform an experimental test.

The fatigue life prediction and dynamic response of the structure was not studied in this work. Due to changes in direction and velocity of the wind, the fatigue analysis is inevitable. Therefore, a fatigue analysis is recommended in order to study the behavior of the PAGV in the real environmental conditions.

Another very important issue is to perform a modal analysis. For the structures exposed to dynamic loads like strong winds, performing modal analysis to obtain the natural frequencies and mode shapes is inevitable. Generally, the natural frequency depends on the shape and supports of the structure. To avoid any resonance the modal analysis is required.

Designing a mechanism in order to adjust the vane angles is an effective way to capture more wind and efficiently guide the wind stream. Such a mechanism will not only increase the performance of the guide vane but also make it more interesting to be used in the market.

Using the uniform strength vanes in order to overcome the large deflection appeared on the middle of the vanes has the potential of reducing the total weight. Further analysis is needed to find the minimum dimension of the uniform strength vane which maintains the lowest possible weight of the PAGV. The effects of uniform strength vane, which is inspired from the airfoil or turbine blade on the wind stream, and the efficiency of the PAGV is a matter of interest.

REFERENCES

- Abe, K., Nishida, M., Sakurai, A., Ohya, Y., Kihara, H., Wada, E., & Sato, K. (2005). Experimental and numerical investigations of flow fields behind a small wind turbine with a flanged diffuser. *Journal of Wind Engineering and Industrial Aerodynamics*, 93(12), 951-970. doi: 10.1016/j.jweia.2005.09.003
- Abuelsamid, S. (2010). Highway wind turbines to capture energy from passing vehicles Retrieved 20/6/2011, <http://green.autoblog.com/2007/05/01/highway-wind-turbines-to-capture-energy-from-passing-vehicles/>
- Ackermann, T. (Ed.). (2005). *Wind power in power systems*. Chichester: John Wiley and Sons Ltd.
- Administration, F. A. (2009). *Pilot's Handbook of Aeronautical Knowledge*. Washington D.C.: United States Government Printing Office.
- Alam, M. J., & Iqbal, M. T. (2009). *Design and development of hybrid vertical axis turbine*. Paper presented at the Canadian Conference on Electrical and Computer Engineering, St. John's, NL.
- Altan, B. D., Atılgan, M., & Özdamar, A. (2008). An experimental study on improvement of a Savonius rotor performance with curtaining. *Experimental Thermal and Fluid Science*, 32(8), 1673-1678.
- ASM, I. (2002). *Atlas of stress-strain curves*. Materials Park, OH: ASM International.
- Bahaj, A. S., & James, P. A. B. (2007). Urban energy generation: The added value of photovoltaics in social housing. *Renewable and Sustainable Energy Reviews*, 11(9), 2121-2136.
- Bakos, G. C., & Tsagas, N. F. (2002). Technical feasibility and economic viability of a small-scale grid connected solar thermal installation for electrical-energy saving. *Applied Energy*, 72(3-4), 621-630.
- Bechly, M. E., & Clausen, P. D. (1997). Structural design of a composite wind turbine blade using finite element analysis. *Computers & Structures*, 63(3), 639-646.
- Bet, F., & Grassmann, H. (2003). Upgrading conventional wind turbines. *Renewable Energy*, 28(1), 71-78.
- Brandt, A. M. (Ed.). (1986). *Criteria and methods of structural optimization*. Hingham, MA: Kluwer Academic Publishers.
- Breslow, P. B., & Sailor, D. J. (2002). Vulnerability of wind power resources to climate change in the continental United States. *Renewable Energy*, 27(4), 585-598.

- Bullock, M., & Musgrove, P. J. (1987). *The effects of turbulence spectra and load profiles on the operation of a modeled 60 kW wind/diesel system*. Paper presented at the 9 th BWEA Wind Energy Conference, Edinburgh, UK.
- Burton, T. (2001). *Wind energy: handbook*. West Sussex: John Wiley and Sons Ltd.
- Cassedy, E. S. (2000). *Prospects for sustainable energy: a critical assessment*. New York, NY: Cambridge University Press.
- Chino, M. (2008). Anara Tower: Dubai's Titanic Turbine-Shaped Superstructure. Retrieved 15/7/2010, from inhabitat <http://inhabitat.com/anara-tower-by-atkins-design-studio/>
- Chong, W. T. (2009). *An innovative design and energy output estimation of wind-solar hybrid renewable energy generation system with rain water collection feature*. Paper presented at the International Conference on Advances in Mechanical Engineering ICAME, Universiti Teknologi Mara.
- Chou, J.-S., & Tu, W.-T. (2011). Failure analysis and risk management of a collapsed large wind turbine tower. *Engineering Failure Analysis*, 18(1), 295-313.
- Christensen, R. M. (2011). Is it Stress or Strain That Causes Failure Retrieved 7/8/2011, from <http://www.failurecriteria.com>
- Colaciti, A. K., Valdés López, L. M., Navarro, H. A., & Cabezas-Gómez, L. (2007). Numerical simulation of a radial diffuser turbulent airflow. *Applied Mathematics and Computation*, 189(2), 1491-1504. doi: 10.1016/j.amc.2006.12.029
- Crespo, A., Hernández, J. and Frandsen, S. (1999), Survey of modelling methods for wind turbine wakes and wind farms. *Wind Energy*, 2: 1–24.
- De Klerk, H. J., & De Villier, R. C. (1984). The properties and welding of Supraform TM steel. *Journal of the South African Institute of Mining and Metallurgy*, 84(12), 381-387.
- Dobrev, I., & Massouh, F. (2011). CFD and PIV investigation of unsteady flow through Savonius wind turbine. *Energy Procedia*, 6, 711-720.
- Du, L., Lee, J.-H., & Kim, Y.-C. (2009). Power prediction of darrieus type wind turbine considering real air velocity on the wind turbine blade. Retrieved 10/7/2011, from School of mechanical engineering, <http://www.eepe.murdoch.edu.au/resources/info/NSWTC/install.html>
- Duquette, M. M., & Visser, K. D. (2003). Numerical Implications of Solidity and Blade Number on Rotor Performance of Horizontal-Axis Wind Turbines. *Journal of Solar Energy Engineering*, 125(4), 425-432.
- Einberg, G., Hagström, K., Mustakallio, P., Koskela, H., & Holmberg, S. (2005). CFD modelling of an industrial air diffuser--predicting velocity and temperature in the

near zone. *Building and Environment*, 40(5), 601-615. doi: 10.1016/j.buildenv.2004.08.020

- Eke, R. K., O; Ulgen, K. (2005). Optimization of a Wind/PV Hybrid Power Generation System. *International Journal of Green Energy*, 2(1), 57-63.
- El Kasmi, A., & Masson, C. (2008). An extended k- ϵ model for turbulent flow through horizontal-axis wind turbines. *Journal of Wind Engineering and Industrial Aerodynamics*, 96(1), 103-122.
- Elchazly , N. (1993). Static and dynamic analysis of wind turbine blades using the finite element method. *Renewable Energy*, 3, 705-724.
- Elhadidy, M. A. (2002). Performance evaluation of hybrid (wind/solar/diesel) power systems. *Renewable Energy*, 26(3), 401-413.
- Engineers, I. o. E., Physics, A. I. o., INSPEC, & Engineering Information, I. (1980). *Science abstracts: Physics abstracts*. Washington, DC: Institution of Electrical Engineers.
- Foreman, K. M., Gilbert, B., & Oman, R. A. (1978). Diffuser augmentation of wind turbines. *Solar Energy*, 20(4), 305-311.
- Fujisawa, N. (1996). Velocity measurements and numerical calculations of flow fields in and around Savonius rotors. *Journal of Wind Engineering and Industrial Aerodynamics*, 59(1), 39-50.
- Fujisawa, N., & Gotoh, F. (1992). Visualization study of the flow in and around a Savonius rotor. *Experiments in Fluids*, 12(6), 407-412.
- Gasch, R. (1982). *Wind turbine generators*. USA: MIT Press.
- Ghasemnejad, H., Occhineri, L., & Swift-Hook, D. T. (2011). Post-buckling failure in multi-delaminated composite wind turbine blade materials. *Materials & Design*, 32(10), 5106-5112.
- Gipe, P. (1998). Comments on the Vortec diffuser augmented turbine. Retrieved 15/7/2010, from wind-works <http://www.wind-works.org/articles/vortec.html>
- Gupta, R., Biswas, A., & Sharma, K. K. (2008). Comparative study of a three-bucket Savonius rotor with a combined three-bucket Savonius-three-bladed Darrieus rotor. *Renewable Energy*, 33(9), 1974-1981.
- Habali, S. M., & Saleh, I. A. (2000). Local design, testing and manufacturing of small mixed airfoil wind turbine blades of glass fiber reinforced plastics: Part I: Design of the blade and root. *Energy Conversion and Management*, 41(3), 249-280.
- Hansen, M. O. L., Sorensen, N. N. and Flay, R. G. J. (2000). Effect of Placing a Diffuser around a Wind Turbine. *Wind Energy*, 3, 207-213.

- Hau, E. (2006). *Wind turbines: fundamentals, technologies, application, economics*. Berlin: Springer.
- Hibbeler, R. C. (2011). *Mechanics of Materials*. Singapore: Pearson Education South Asia Pte. Ltd.
- Hu, S.-Y., & Cheng, J.-H. (2008). Innovatory designs for ducted wind turbines. *Renewable Energy*, 33(7), 1491-1498.
- Hutton, D. V. (2003). *Fundamentals of Finite Element Analysis*. New York, NY: McGraw-Hill.
- Igra, O. (1981). Research and development for shrouded wind turbines. *Energy Conversion and Management*, 21(1), 13-48. doi: 10.1016/0196-8904(81)90005-4
- Iskandarani, M., Finite Volume Method, in Numerical Methods in Fluid Dynamics. 2002, University of Miami: Miami. p. 290.
- James, & Petersen, E. L. (1999). *European wind energy conference: wind energy for the next millennium*. Nice: James & James.
- Janajreh, I., R. Qudaih, et al. (2010). Aerodynamic flow simulation of wind turbine: Downwind versus upwind configuration. *Energy Conversion and Management* 51(8): 1656-1663.
- Kentfield, J., Alan, Charles. (1996). *The fundamentals of wind-driven water pumpers*. Amsterdam B.V.: Overseas publishers association
- Kong, C., Bang, J., & Sugiyama, Y. (2004). Structural investigation of composite wind turbine blade considering various load cases and fatigue life. *Energy*, 30(11-12)
- Kuma, H., Takao, M., Beppu, T., Maeda, T., Kamada, Y., & Kamemoto, K. (2008). A Straight-Bladed Vertical Axis Wind Turbine With a Directed Guide Vane: Mechanism of Performance Improvement. *ASME Conference Proceedings*, 2008(48234), 617-623.
- Lilley, G. M., & Rainbird, W. J. (1956). *A preliminary report on the design and performance of ducted windmills*. Cranfield: College of Aeronautics.
- Madsen, P. H., & Frandsen, S. (1984). Wind-induced failure of wind turbines. *Engineering Structures*, 6(4), 281-287.
- McGowan, J. G., & Manwell, J. F. (1998). Hybrid wind/PV/diesel system experiences. *Renewable Energy*, 16(1-4), 928-933.
- McHenry, M. (2010). Vertical Axis Turbines VAWT. Retrieved 5/7/2011, from Murdoch University <http://www.eepe.murdoch.edu.au/resources/info/NSWTC/install.html>

- Mertens, S. (2006). *Wind Energy in the built environment: concentrator effects of buildings*. Brentwood: Multiscience Publishing.
- Miller, F. P., Vandome, A. F., & McBrewster, J. (2010). *Darrieus Wind Turbine*. Mauritius: Alphascript Publishing.
- Nema, P., Nema, R. K., & Rangnekar, S. (2009). A current and future state of art development of hybrid energy system using wind and PV-solar: A review. *Renewable and Sustainable Energy Reviews*, 13(8), 2096-2103.
- Noda, M., & Flay, R. G. J. (1999). A simulation model for wind turbine blade fatigue loads. *Journal of Wind Engineering and Industrial Aerodynamics*, 83(1-3), 527-540. doi: 10.1016/s0167-6105(99)00099-9
- Orosa, J. A., Garcia-Bustelo, E. J., & Perez, J. A. (2009a, 18-20 March 2009). *Climate effects in low speed wind turbine's concentrators*. Paper presented at the International Conference on Power Engineering, Energy and Electrical Drives Lisbon, Portugal.
- Orosa, J. A., Garcia-Bustelo, E. J., & Perez, J. A. (2009b, 18-20 March 2009). *Wind turbine concentrator design based on moist air phase change*. Paper presented at the International Conference on Power Engineering, Energy and Electrical Drives, Lisbon, Portugal.
- Rahimi, M., & Parniani, M. (2009). Dynamic behavior and transient stability analysis of fixed speed wind turbines. *Renewable Energy*, 34(12), 2613-2624.
- Research, A. A. (2010). Help system, *Modeling turbulence*: ANSYS, Inc.
- Righter, R. W. (1996). *Wind energy in America: a history*. Norman, OK: University of Oklahoma Press.
- Shokrieh, M. M., & Rafiee, R. (2006). Simulation of fatigue failure in a full composite wind turbine blade. *Composite Structures*, 74(3), 332-342. doi: 10.1016/j.compstruct.2005.04.027
- Singh, G. (2008). *Exploit Nature-Renewable Energy Technologies*. New Delhi: Aditya Books Pvt. Ltd.
- Spera, D. A. (Ed.). (1994). *Wind turbine technology*. New York: ASME Press.
- Takao, M., Kuma, H., Maeda, T., Kamada, Y., Oki, M., & Minoda, A. (2009). A straight-bladed vertical axis wind turbine with a directed guide vane row — Effect of guide vane geometry on the performance —. *Journal of Thermal Science*, 18(1), 54-57.
- Tina, G., Gagliano, S., & Raiti, S. (2006). Hybrid solar/wind power system probabilistic modelling for long-term performance assessment. *Solar Energy*, 80(5), 578-588.

- Toft, H. S., & Sørensen, J. D. (2011). Reliability-based design of wind turbine blades. *Structural Safety, In Press, Corrected Proof*. doi: 10.1016/j.strusafe.2011.05.003
- Wang, F., Bai, L., Fletcher, J., Whiteford, J., & Cullen, D. (2008). Development of small domestic wind turbine with scoop and prediction of its annual power output. *Renewable Energy*, 33(7), 1637-1651.
- Wang, S.-H., & Chen, S.-H. (2008a). Blade number effect for a ducted wind turbine. *Journal of Mechanical Science and Technology*, 22(10), 1984-1992.
- Wang, S.-H., & Chen, S.-H. (2008b). *The study of interference effect for cascaded diffuser augmented wind turbines*. Paper presented at the The seventh Asia-Pacific conference on wind engineering, Taipei, Taiwan.
- Wijk, V. (1991). *The value of wind energy* Paper presented at the 13th British Wind Energy Association Conference "Wind Energy and the Environment", Swansea, UK

University of Malaya

Appendix A

Mesh dependency

Table A.1: Mesh dependency with respect to number of elements

Element Type	Number of elements	Maximum Stress (MPa)
Tetrahedra	854356	306.06
Tetrahedra	852116	306.87
Tetrahedra	851720	305.11
Tetrahedra	849831	309.82
Tetrahedra	752682	312.48
Tetrahedra	702303	329.30
Tetrahedra	656431	305.21
Tetrahedra	612415	317.49
Tetrahedra	590422	336.12

Mesh dependency

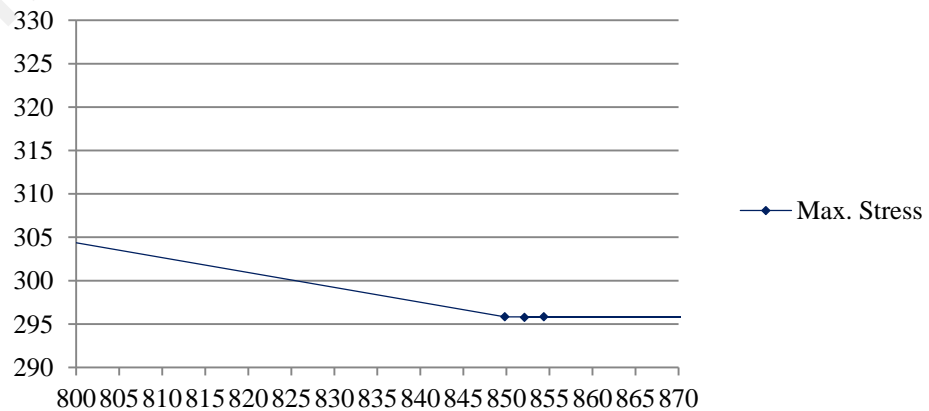


Figure A.1: Element number versus maximum stress (Structural)

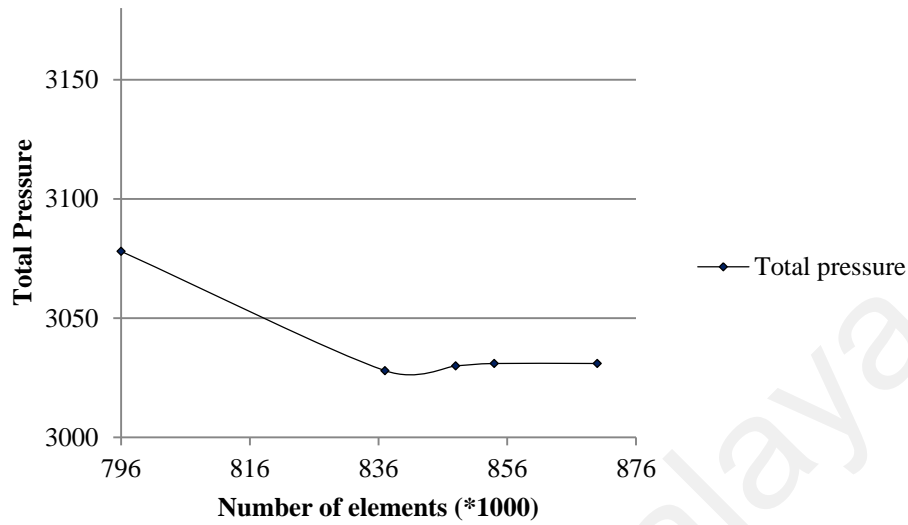


Figure A.2: Element number versus maximum stress (CFD)

Tawau	24.6	26.6	28.1
Subang	29.2	32.1	34.3
Sri Aman	27.6	30.3	32.4
Sitiawan	23.3	25.3	26.7
Sibu	27.0	29.3	31.0
Senai	26.9	29.1	30.7
Sandakan	23.4	25.8	27.7
Petaling Jaya	28.8	31.4	33.4
Muadzam Shah	22.6	24.4	25.8
Miri	26.9	29.0	30.5
Mersing	29.5	32.0	33.8
Melaka	26.7	29.4	31.3
Labuan	26.0	27.7	29.0
Kudat	27.1	29.1	30.6
Kuala Terengganu	25.5	27.2	28.5
Kuantan	27.5	29.8	31.6
Kluang	29.6	32.6	34.9
Kuala Krai	27.2	29.5	31.3
Kuching	29.5	32.6	34.9
Kota Bahru	30.0	32.4	34.2
Kota Kinabalu	28.3	30.5	32.2
Ipoh	30.6	33.5	35.7
Chuping	23.8	25.6	27.0
Cameron Highlands	25.2	26.8	28.0
Butterworth	24.6	26.4	27.7
Batu Embun	25.3	27.5	29.2
Bayan Lepas	25.6	27.5	28.9
Bintulu	23.9	25.6	26.9
Alor Setar	27.2	29.9	31.8

Table A.2: Wind speed for all directions based on three seconds gust wind data

Site in country, or less than 2 km inside town					Site in town, extending ≥ 2 km upwind from the site			
Effective height H_e : m	Closest distance to sea: km				Effective height H_e : m	Closest distance to sea: km		
	≤ 0.1	2	10	100		2	10	100
2	1.48	1.39	1.35	1.26	2	1.19	1.15	1.07
5	1.65	1.62	1.57	1.46	5	1.51	1.46	1.36
10	1.78	1.78	1.73	1.62	10	1.74	1.69	1.58
15	1.86	1.85	1.82	1.71	15	1.84	1.82	1.71
20	1.90	1.90	1.89	1.77	20	1.89	1.89	1.77
30	1.97	1.96	1.96	1.85	30	1.95	1.96	1.85
50	2.04	2.04	2.04	1.95	50	2.02	2.03	1.95
100	2.12	2.12	2.12	2.07	100	2.11	2.11	2.07

Table A.3: Terrain and structure factor S_p (BS-6399, Part: 2)

Appendix B

Important Simulation Steps

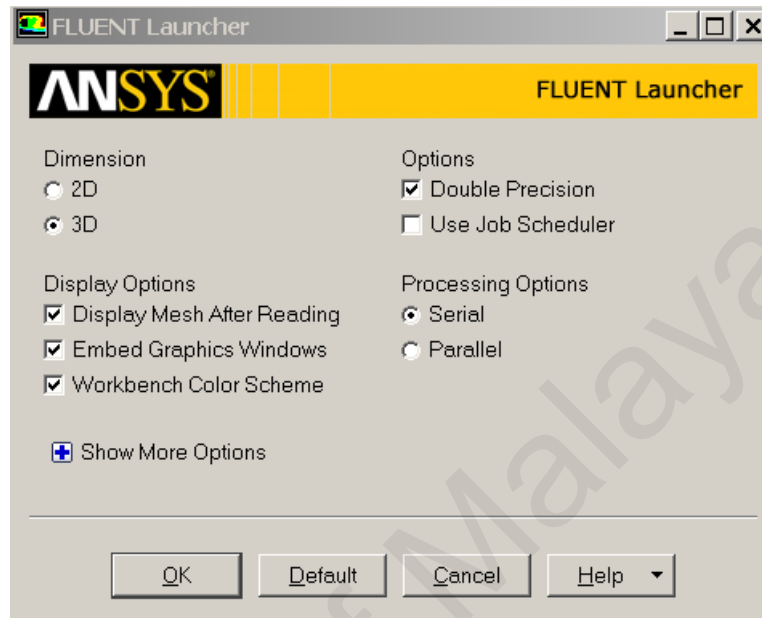


Figure B.1: Starting the Fluent

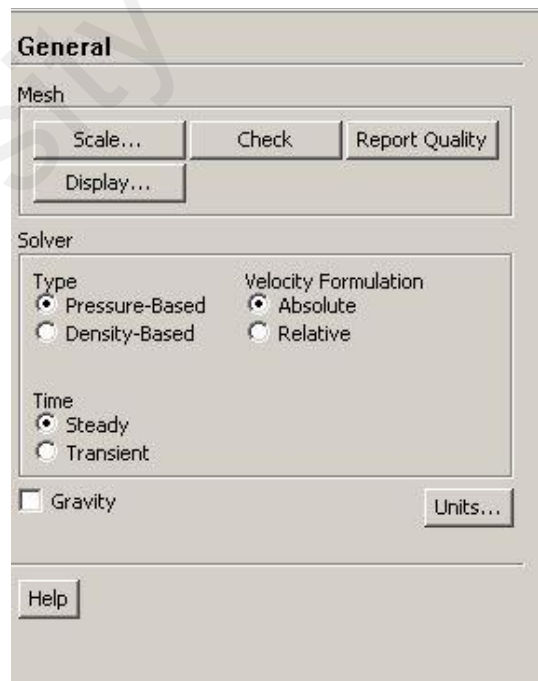


Figure B.2: Set up the Fluent solver

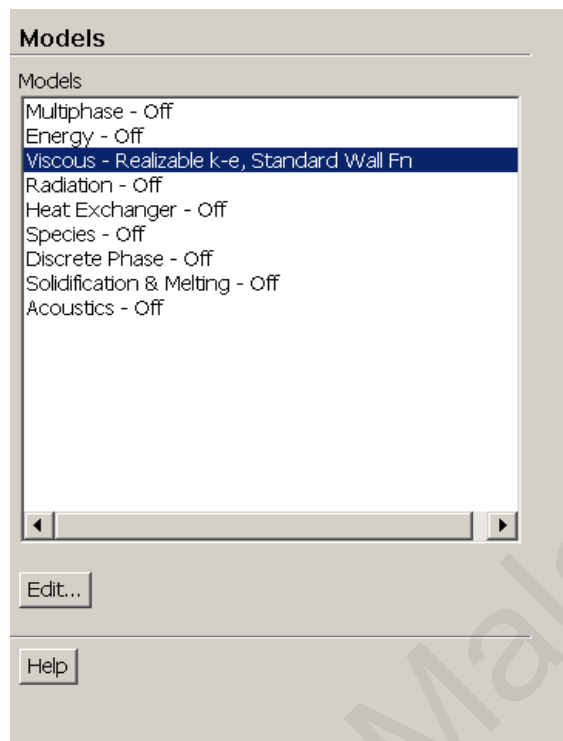


Figure B.3: Selecting the appropriate viscous model

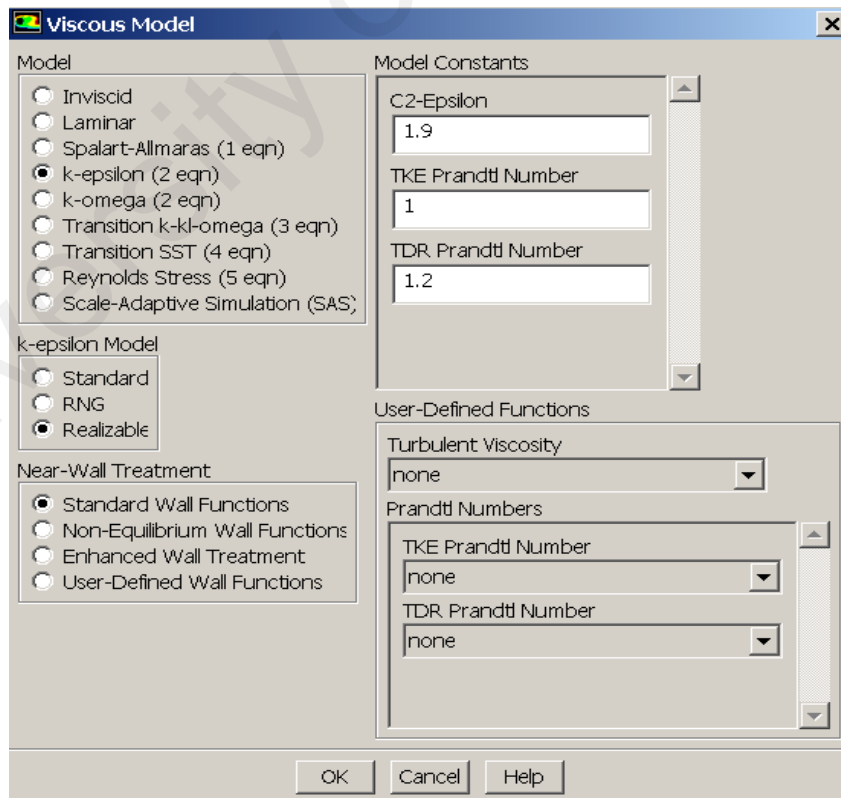


Figure B.4: Setting the Realizable k-ε model



Figure B.5: Setting the boundary conditions

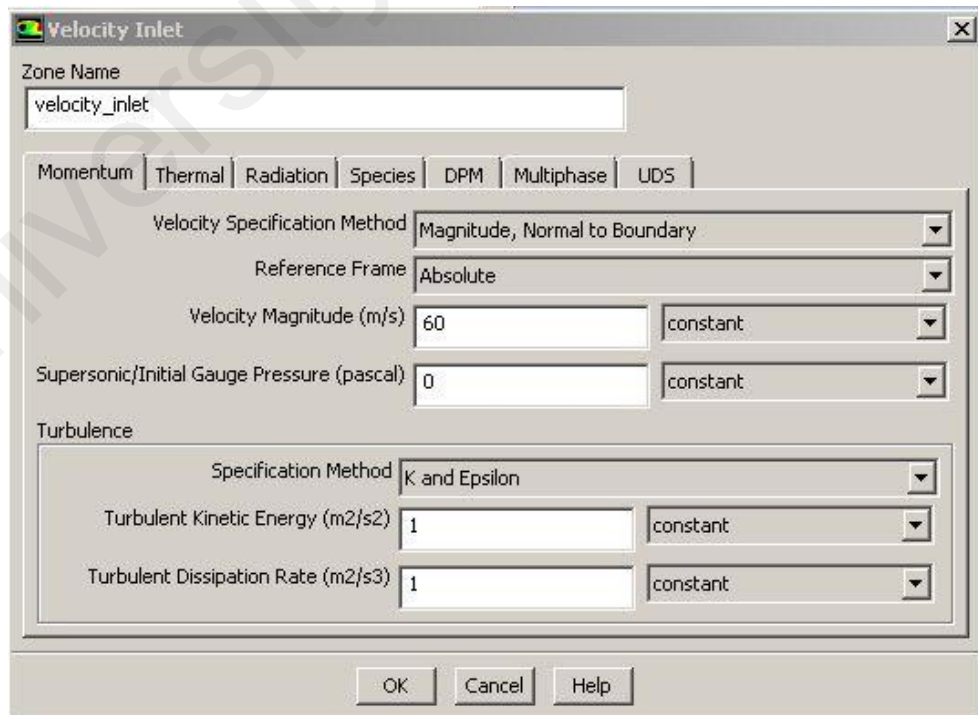


Figure B.6: Define the air velocity magnitude

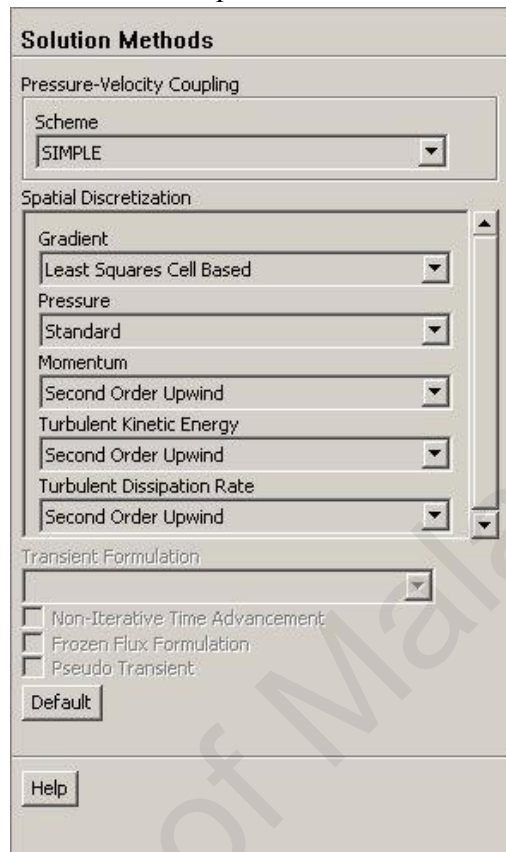


Figure B.7: Choosing the solution schemes

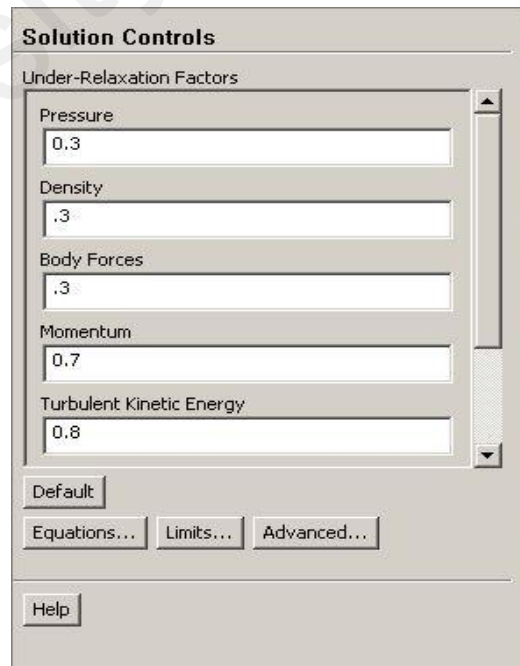


Figure B.8: Define under relaxation factors

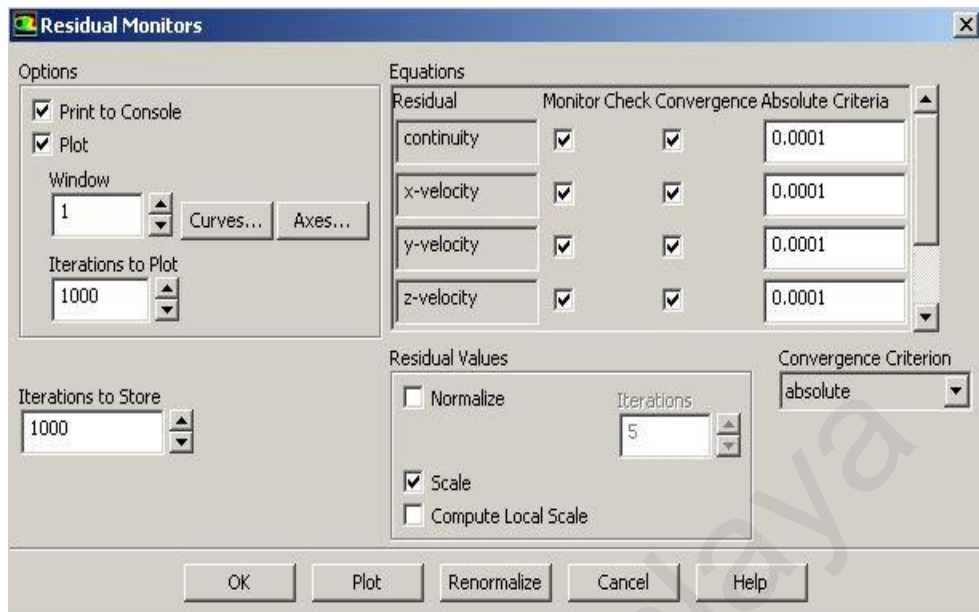


Figure B.9: Define the convergence absolute criteria

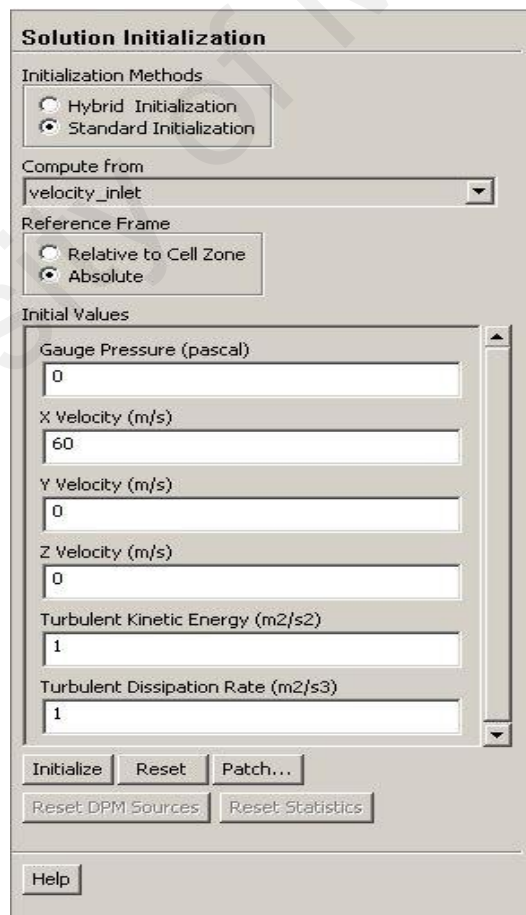


Figure B.10: Initialize the solution

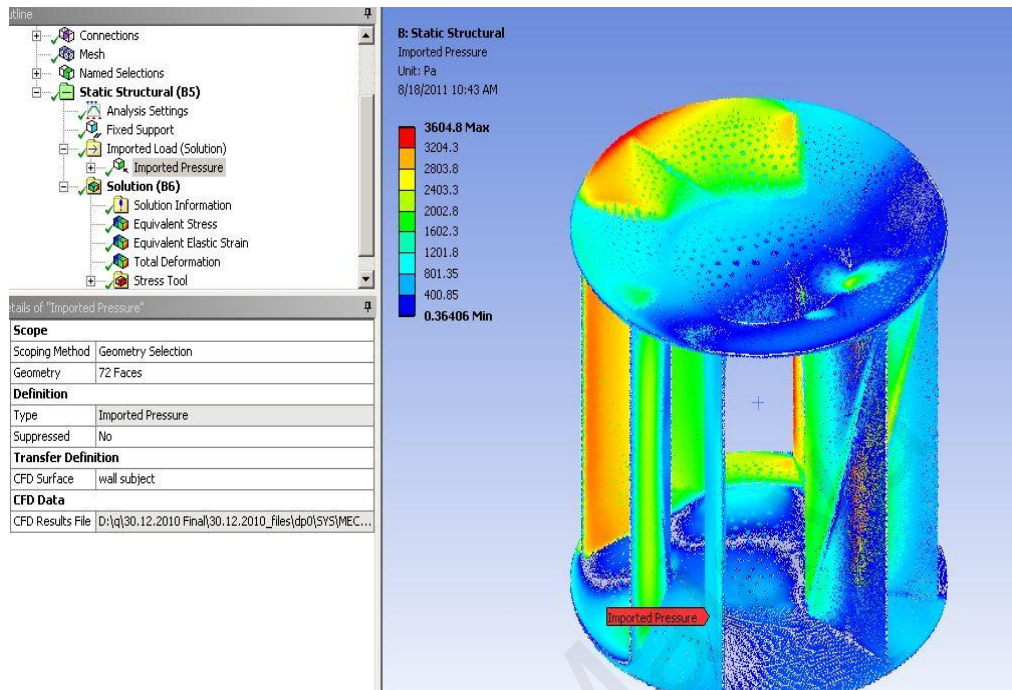


Figure B.11: Transferring the pressure profile to the structural solver

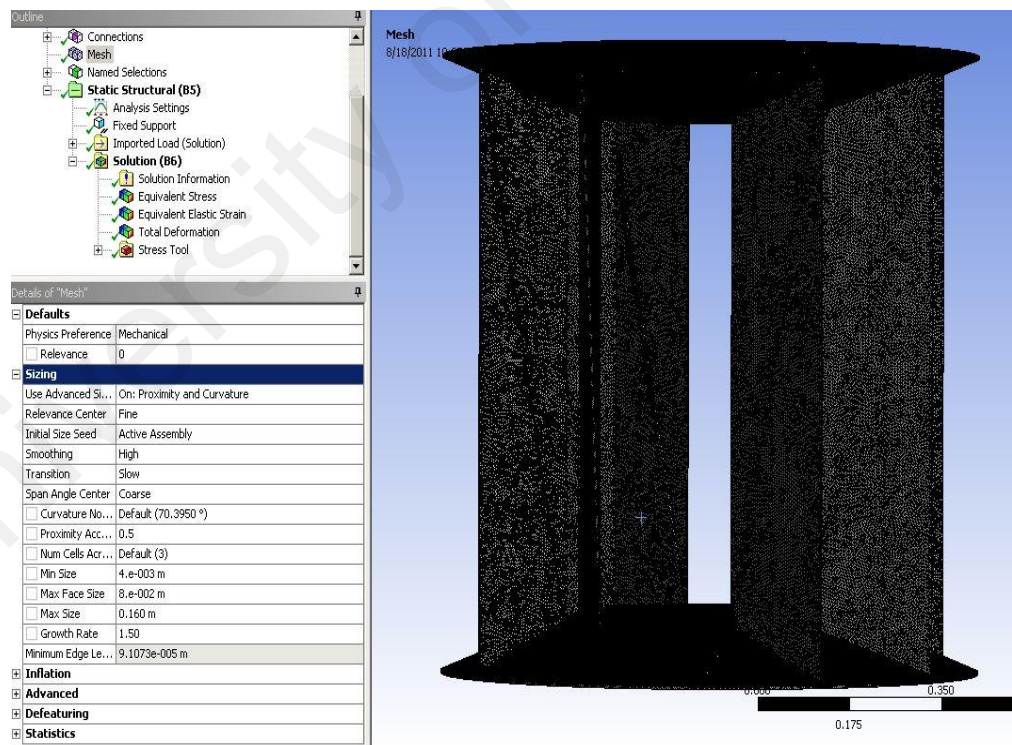


Figure B.12: Generating mesh for the PAGV

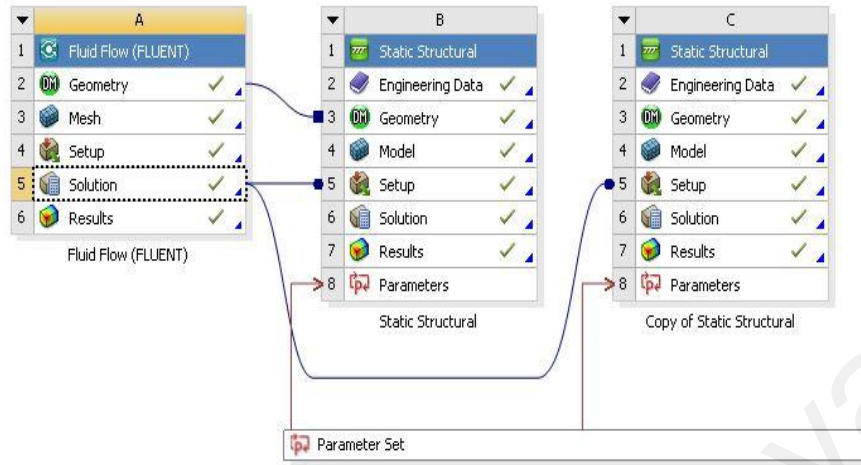


Figure B.13: Project layout

University of Malaya